# Accepted Manuscript

Infrared thermography: A non-invasive window into thermal physiology

Glenn J. Tattersall

Please cite this article as: Tattersall, Glenn J., Infrared thermography: A non-invasive window into thermal physiology, *Comparative Biochemistry and Physiology, Part A* (2016), doi: 10.1016/j.cbpa.2016.02.022

# Infrared thermography: A non-invasive window into thermal physiology

**Invited Review for a special issue on non-invasive approaches to field physiology**

Glenn J. Tattersall

Department of Biological Sciences,

Brock University,

St. Catharines, Ontario, Canada

Department of Biological Sciences

Brock University

St. Catharines, Ontario,

L2S 3A1, Canada

Tel. 905 688 5550 ext. 4815

e-mail:  gtatters@brocku.ca

## Abstract

Infrared thermography is a non-invasive technique that measures mid to long-wave infrared radiation emanating from all objects and converts this to temperature. As an imaging technique, the value of modern infrared thermography is its ability to produce a digitized image or high speed video rendering a thermal map of the scene in false colour. Since temperature is an important environmental parameter influencing animal physiology and metabolic heat production an energetically expensive process, measuring temperature and energy exchange in animals is critical to understanding physiology, especially under field conditions. As a non-contact approach, infrared thermography provides a non-invasive complement to physiological data gathering. One caveat, however, is that only surface temperatures are measured, which guides much research to those thermal events occurring at the skin and insulating regions of the body. As an imaging technique, infrared thermal imaging is also subject to certain uncertainties that require physical modeling, which is typically done via built-in software approaches. Infrared thermal imaging has enabled different insights into the comparative physiology of phenomena ranging from thermogenesis, peripheral blood flow adjustments, evaporative cooling, and to respiratory physiology. In this review, I provide background and guidelines for the use of thermal imaging, primarily aimed at field physiologists and biologists interested in thermal biology. I also discuss some of the better known approaches and discoveries revealed from using thermal imaging with the objective of encouraging more quantitative assessment.

## 1. Introduction

Infrared thermography (IRT) emerged as a technology in the 1960s developed by the United States military initially for nighttime surveillance and heat signature detection (Rogalski, 2012). With expansion of access to non-military, scientists, and civilians, it is now used extensively in numerous fields, including law enforcement, engineering, building assessment, medical imaging, as well as in biological (Berz and Sauer, 2007; Kouba, 2005; McCafferty, 2007) and ecological applications (Boonstra et al., 1994; Rodriguez et al., 2011). More recent advances in thermal imaging have capitalized on the sensitivity of this technique for assessing relative miniscule changes in temperature that underlie changes in peripheral blood flow, which has led to repeated suggestions that thermal imaging would be a viable diagnostic tool in veterinary and human medicine (Jones, 1998; Turner, 2001), sports medicine (Al-Nakhli et al., 2012; Hildebrandt et al., 2010), and breast cancer detection (Kerr, 2004), to name a few. In terms of field applications, landscape ecologists and agricultural science have been advancing the discipline through the use of thermal imaging in combination with unmanned aerial vehicles to reconstruct thermal heterogeneity at a local scale (Faye et al., 2015), suggesting a very innovative approach to acquiring geo-tagged thermal information on organisms in their natural environments.

As an imaging technology, IRT has numerous advantages resulting from its non-invasive and non-contact approach (Usamentiaga et al., 2014). In this way, thermal information can be assessed from a distance, a valuable feature for field biology, without the need for surgical interventions or handling that have prolonged effects on body temperature. For example, in laboratory rodents and even in some ectotherms, an emotional fever accompanies handling, leading to an elevation in $T_b$ measurements associated with experimenter handling (Cabanac and Gosselin, 1993; Michel et al., 2003; Thompson et al., 2003). Non-contact methods of measuring temperature like IRT obviate this experimental confound, although with the sacrifice of information on core body temperature. IRT also produces a real-time, two-dimensional image of the temperature of an environment, allowing areas within the image to be compared offline for temperature differences. These temperature differences arise from numerous physical phenomena, including evaporation, differential thermal conduction, and altered surface physical

phenomena (*e.g.,* emissivity).  Since IRT provides real-time thermal information, events can be monitored from rapidly changing objects within the field of view.  As an imaging technique, one final advantage offered by IRT is the lack of harmful radiation or the addition of contrasting dye injections, which makes it appropriate for repeated usage with minimal preparation (Usamentiaga et al., 2014).

The goal of this review is to provide comparative and field physiologists with a introductory guide to the challenges, pitfalls, and utility of IRT, and to encourage more quantitative research into non-invasive thermophysiology.  To do this, I will provide a basic background to the physics and mathematical aspects underlying thermography, some practical considerations important when using thermography, and examples of the application of IRT to animal physiology. For a more complete background to the mathematical and theoretical physical explanations, readers are advised to consult numerous technical references (Lane et al., 2013; Matis et al., 2006; Minkina and Dudzik, 2009; Proulx, 2011; Rogalski, 2012; Usamentiaga et al., 2014), as well as numerous reviews on the topic dealing specifically with biological examples (McCafferty, 2007; Speakman and Ward, 1998; Tattersall and Cadena, 2010).  My objective in this overview is to share experiences with how IRT has been applied to thermophysiology, comparative physiology, ecophysiology and evolutionary physiology.  I provide guidelines and recommendations for those interested in adopting thermal imaging into their research, as well as cautionary advice on what may work with present day technology.  This advice is informed by commonly asked questions, such as whether IRT can measure the temperature of an animal underwater (Lathlean and Seuront, 2014), whether IRT can see through walls and glass, or whether IRT can obtain deep body temperature measurements.  The answer to all three of these questions is "no" on the basis of how objects interact with the infrared radiation being detected, and suggests that the basics of thermal imaging are not well appreciated by many biologists.  Therefore, this review will provide methodological guidance rather than a review of the literature; however, I will highlight a number of applications of IRT in the context of comparative thermophysiology.

## 2.1. Background and Theory

The discovery of infrared radiation began with William Herschel's (1738-1722) experiments into "dark light", that portion of the sun's electromagnetic spectrum that was invisible to the naked eye.  Following on from Newton's discovery that visible light could be refracted into distinct colour bands, Herschel recorded the rise in temperature produced by each "band of colour" of visible light and noticed that the "dark light" just beyond the range of red also produced heat, providing the first evidence for an infrared form of light.  The fact that this near visible light – Herschel called them "calorific rays" - followed the same optical principles of visible light and other forms of radiation was the evidence required for inferring a thermal form of electromagnetic radiation (Rogalski, 2012).  The visible light spectrum is restricted to a narrow range of wavelengths (390-700 nm), whereas the spectrum of electromagnetic radiation described as infrared is a wide range, starting at 700 nm (just beyond the visible range) up to 1 mm wavelengths.  A small portion of this range is referred to as the thermal infrared range (8-15 μm) for its primary use in infrared thermal imaging.

A thermogram (or thermograph) is simply an image, impression, or visual representation of a scene's temperature.  The first thermograms produced pre-dated thermal imaging devices, and capitalized on thermally sensitive rates of evaporation of water or oil. Hippocrates (300 BCE) is credited with describing an early version of a two-dimensional rendition of skin temperature by using a moist, linen cloth covering an area of skin to produce an impression of surface temperatures via the change in cloth colour (Otsuka and Togawa, 1997). Years later (in the 1800s), by inducing a gradient of heat across the surface of a thin oil film, William Herschel showed how a visual interference pattern would be revealed by the differential rates of evaporation, thereby producing an "image" of temperature on the surface (Rogalski, 2012).  The modern usage of the term thermograph has come to be associated with the rendering of a false colour image of the thermal environment, and so the thermogram, which is often called a "thermal image", provides a visual rendering of the energy emitted, transmitted, and reflected by an object and its environment.

All objects, including animals, consist of matter in random motion, containing kinetic heat (sometimes referred to as true heat); objects above absolute zero Kelvin

contain this random motion, which leads to particles colliding, changing their energy state and leading to the release in electromagnetic radiation. Radiant flux ($\Phi$) refers to the radiative energy that exits or is emitted by an object and is usually measured in Watts. Since there is typically a strong positive relationship between an object's true kinetic temperature (reflective of the energy state of the object) and the amount of radiant flux radiated from the object (*i.e.,* from a blackbody), radiometers that detect the radiant energy can be used to distantly estimate the object's true kinetic temperature. The relationship between radiant energy and object temperature is not definitive, however; the radiant temperature is usually slightly lower than the true kinetic temperature due to differences in object emissivity (see below).

## 2.2. Blackbody Radiation

An ideal blackbody is an object that completely absorbs all of the electromagnetic radiation that it receives at every wavelength. This same body also radiates energy at a maximum potential rate per unit area and unit wavelength at any given temperature. The term black has not bearing on the object's colour, *per se*, except in how it describes how a blackbody behaves similarly with respect to all wavelengths. No objects in nature are actually true black bodies, however the insights from Planck's law that a blackbody radiator emits a distinctive and predictable radiation with respect to its own temperature is central to how infrared thermal imaging operates. All objects that are above absolute zero Kelvin emit electromagnetic radiation. This is essentially summarized in Planck's law and can be more readily understood by expressing the equation for blackbody radiation. A physical blackbody is an "ideal radiator", wherein the spectral radiance, *I*, at a given wavelength and absolute temperature can be expressed through the following equation derived from Planck's law:

$$I(\lambda, T) = \frac{2hc^2}{\lambda^5} \cdot \frac{1}{\left(e^{\frac{hc}{\lambda kT}} - 1\right)}$$

where $I(\lambda,T)$ is the energy per unit time radiated per unit area of emitting surface per solid angle per unit wavelength at known absolute temperature *T* (Kelvin), *h* is the Planck constant, *k* is the Boltzmann constant, and *c* is the speed of light in a vacuum (Figure 1). This relationship produces a curvilinear relationship where spectral radiance rises to peak

at a characteristic wavelength related to blackbody temperature. Although biologists and physiologists tend to utilize the Celsius scale for temperature, in all uses of temperature involving physical relationships, degrees Kelvin are used.

## 2.3. Wein's Law and Electromagnetic Radiation

Wien's displacement law describes how blackbody radiation spectral curves are related to absolute temperature. True blackbody temperature can be related to the peak spectral exitance (*i.e.,* dominant wavelength, $\lambda_{max}$, m) in such a way that the wavelength where the intensity (per unit wavelength) of radiation produced by a blackbody is maximal according to the following equation:

$$\lambda_{max} = \frac{b}{T}$$

where *b*, Wien's displacement constant is equal to $2.8977721 \times 10^{-3}$ K·m. The effects of Wein's law are readily apparent in the orange glow of the burning embers of a fire, which at 1000-1400K produce peak spectral radiance outside of the visible range, but with sufficient overlap at the long visible wavelengths, bestowing its slight orange-red hue. The dominant wavelength also allows thermal imaging manufacturers to design imaging sensors that best match the range of temperatures being examined. Since the sensors absorb infrared radiation within limited wavelength ranges according to the material they are made from, the sensitivity of a given sensor needs to be matched to the range of temperatures being examined for maximum signa-to-noise ratio. For example, an object that is 800K would have a dominant wavelength of 3.62 μm; medium wave infrared radiation (MWIR; typically 3 to 5 μm) sensors would be most appropriate. Animals cannot tolerate or generate such high temperatures and so for biological applications long wave infrared radiation (LWIR; 8 to 12 μm) sensors are typically used; an animal surface temperature of 30°C (303K) would have a peak wavelength of 9.56 μm which is well within the range of sensor sensitivity of LWIR thermal imagers.

## 2.4. Kirschoff's Radiation Law

At a given wavelength, incident radiation arriving at an object is either transmitted, absorbed, or reflected, accordingly summarized in the following equation of total radiative flux (*Φ;*□□□□:

$$\phi_{incident} = \phi_{transmitted} + \phi_{absorbed} + \phi_{reflected}$$

If expressed as a fraction of the incident radiation, this leads to the following summation:

$$\tau + \alpha + \rho = 1$$

where $\tau$, $\alpha$, and $\rho$ are the transmittance, absorptance, and reflectance coefficient, respectively, and are properties of the material. Typically, in most materials, including biological surfaces, no radiant flux occurs through the material, which means that $\tau$ equals 0, and the relationship can be simplified to:

$$\alpha + \rho = 1$$

which states that incident radiation is either absorbed or reflected. In terms of understanding emitted radiation, Kirchhoff's Radiation law summarises what are complex interactions between radiative heat exchange. Kirschoff surmised that at thermodynamic equilibrium (*i.e.,* steady state) an ideal blackbody (which reflects zero radiation) absorbs all incoming radiation and because of the conservation of energy, it would have to emit the equivalent amount of radiation according to the Stefan-Boltzmann relationship, otherwise it would absorb more radiation than it loses and increase in temperature (a violation of the second law of thermodynamics). Thus, at thermodynamic equilibrium, the total amount of emitted radiation must be equivalent to the absorbed radiation and therefore, emittance is equal to absorptance. Another consequence of this relationship is that emittance and reflectance are inversely related. Indeed, Kirschoff's radiation law has often been re-phrased as: "good absorbers are good emitters and good reflectors are poor emitters", which is formulaically expressed as:

$$\varepsilon + \rho = 1$$

One final, but important consequence of these physical laws of relevance to IRT is that no physical body can emit more radiation than a blackbody, since emissivity is the ratio of the body's radiant flux ($M_r$) to that of a blackbody at the same temperature ($M_b$):

$$\varepsilon = \frac{M_r}{M_b}$$

This relationship sets an upper limit to the radiation that an object can emit, and is central to how thermal imagers are calibrated in order to estimate object temperatures.

## 2.5. Stefan-Boltzmann Law and Infrared Radiation

Integrating beneath the curve for spectral radiance described by Planck's law (Figure 1) reveals that the total spectral radiant exitance per unit area of a surface of a blackbody is directly proportional to the 4$^{th}$ power of the absolute temperature ($T$) of the blackbody in the following manner:

$$M_b = A\sigma T^4$$

where $\sigma$ is the Stefan-Boltzmann constant ($5.66697 \times 10^{-8}$ W m$^{-2}$ K$^{-4}$), and $A$ is the surface area (m$^2$). This exitance can also be thought of as the ability of objects to emit electromagnetic radiation, where an $\varepsilon=1$ is the maximum capacity equivalent to a blackbody radiator. All animals emit radiation to their environment, but are simultaneously absorbing radiation from their environment, and thus, the net power ($P$) radiated, following Newton's second law of thermodynamics, is the difference between that emitted by the animal and that absorbed from the environment:

$$P_{net} = P_{emitted} - P_{absorbed} = A\sigma\varepsilon(T_{animal}^4 - T_{environment}^4)$$

The above relationship assumes, however, that emissivity is constant across all wavelengths of radiation absorbed, and that absorbance is equal to emissivity at thermodynamic equilibrium (Kirschoff's radiation law). In natural situations, radiation is typically absorbed at the shorter wavelengths of visible and ultraviolet light from the sun, while body heat is exchanged with the environment at longer wavelengths, and thus emissivity is not constant across all wavelengths, although within the infrared region of wavelengths, most biological materials appear to have an approximately constant emissivity.

## 2.6. Emissivity

The emissivity of a material influences how that object interacts and emits radiation (Figure 2). The widely used term "emissivity" is technically a physical property of an ideal material, whereas, emittance is the comparable term for real world objects, due to surface imperfections and viewing angle; for historical reasons, in the field of thermography, emissivity has become the commonplace term used to describe the proportion of blackbody radiation an object emits (Holst, 2000). Most objects selectively radiate electromagnetic radiation, with wavelength specific emissivities from 0 to <1. In

contrast, a grey body is simply an object with constant emissivity (<1) across all wavelengths under consideration, which is more typically used in thermal modeling. Indeed, thermal imaging assumes that most objects being examined behave more like grey bodies with respect to infrared radiation, and thus typically a single emissivity value is assigned or estimated. For example, distilled water has an emissivity very close to one (0.99) over the wavelength ranges of 8 to 14 μm, whereas polished aluminum has a very low emissivity (0.08; *i.e.,* high reflectance). For biological tissues, convention has been to use an $\varepsilon$ value of 0.95 to 0.98, depending on the source (Best and Fowler, 1981; Hammel, 1956). The exact value used is unlikely to produce much error (Figure 3), since most biological surfaces consist of similar substances, namely water and organic matter. If an exact determination of $\varepsilon$ is not possible or practical (*i.e.,* for biological tissues temperatures may not be accurately modified by artificial means), $\varepsilon$ can be approximated by comparing surface temperature estimates to substances of known $\varepsilon$. Numerous paints or substances have $\varepsilon$ values close to 0.95. Most thermal imaging companies recommend using black electrical tape ($\varepsilon = 0.95$-0.97) adhered to the surface of interest, which is then heated up to a temperature ~40 degrees above ambient temperature. The thermal imaging software can then be used to "solve" for the apparent emissivity of the surface by comparing the temperature of the electrical tape with the surface temperature of interest and altering apparent emissivity until the two temperatures match one another. For biological tissues, this solution is a challenge since it involves destructive sampling of the surface, and is impossible to perform on the skin of living animals due to convective and conductive heat exchange from the circulating blood beneath. For fur or feathers, however, this could be conducted under controlled conditions (Figure 3). Typically, however, since biological tissues are composed primarily of water and organic compounds, emissivity values >0.95 are often assumed, with 0.98 being widely reported as appropriate for human skin.

## *2.7. Background Reflectance*

Every thermographic scene is potentially influenced by the reflected radiation, since natural objects do not behave precisely like black bodies. In terms of IRT, the background reflectance temperature used in mathematical models to estimate surface

temperature refers to the aggregate temperature of the environment that impinges upon the object of interest. For biological objects, which are grey bodies ($\varepsilon < 1$), a portion (*i.e.,* $1 - \varepsilon$) of the radiation arriving to the thermal imaging device would be resulting from the background environment itself. Most environments are not uniform in temperature, so this background temperature can be difficult to estimate accurately. In some applications, especially indoors, air temperature is taken as background temperature (FLIR, 2007). In outdoor applications, it would be more appropriate to use the average sky temperature. Cloud cover and time of day will impact these estimates. Nevertheless, since emissivity of biological tissues is high, the influence of background reflectance on the estimated temperature is reasonably low, producing a maximum error in absolute temperature that is proportional to the reflectivity of the object ($1-\varepsilon$), which is about 5%.

## *2.8. Atmospheric and Distance Effects*

Of the atmospheric gases, it is primarily carbon dioxide, ozone, and water vapour, that influence the radiant energy detected by the thermal imaging sensor (Sheahen, 1983). If working within a vacuum, then the absorption of infrared radiation would be zero; however, most applications in thermal physiology involve working at prevailing atmospheric conditions. For the range of wavelengths detected by LWIR cameras, water vapour is the most important absorber of radiation (Holst, 2000). Infrared absorbance by water molecules in the atmosphere can attenuate the radiation by up to 10% at 100 m and over 90% at 10 km path lengths. The longer the distance, the more atmospheric interference. For most biological applications, measurements are likely to be conducted between 1 and 100 meters, rather than at the kilometer scale, however, humidity will still influence measurements and should be recorded or estimated if possible. Most thermal imaging software incorporates empirical atmospheric transmission curves for estimating the loss of signal resulting from the water vapour pressure and distance (Holst, 2000). In addition to atmospheric path effects, with digital imaging the minimum resolvable temperature is inherently dependent on distance (Faye et al., 2016), and should also be considered (see Section 3.4).

## 2.9. Window Transmission

On occasion, an application demands that the thermal camera be operated in an environment separated or segregated from the animal. In particular, situations where space constraints prevent the thermal camera from being placed in close proximity to the animal may arise, especially when working in small or enclosed environments. Likewise, research questions where the local gas environment around the animal needs to be maintained in a closed environment, as in applications involving respirometry (Dzialowski et al., 2014; Tattersall and Milsom, 2003), require that infrared transparent windows be used in order to allow detection of the IR from the animal. Inexpensive solutions involve very thin (<10-15 μm) plastics (*e.g.,* polyethylene) which may have effective transmission values ($\tau$) between 0.5 to 0.8. While it is possible to account for the loss of object radiation mathematically with thermal imaging software, the camera's radiation is often reflected on the window itself, which interferes with temperature estimates but could be solved with slight changes in viewing angle. Alternative solutions involve deriving empirical calibrations of the thermal image with the IR window in place while presenting objects of independently verified temperatures and emissivities. An apparent temperature estimated through thermography can then be corrected to the expected temperature and used to account for window transmission loss (Dzialowski et al., 2014). The superior solution to the window transmission challenge is to utilize an IR window which is specifically designed to minimize transmission loss. In some cases, transmission levels as high as 0.96 can be achieved with the appropriate materials (FLIR, 2007). There are numerous materials that can be effective windows depending on the application and desired spectral range. For LWIR and biological applications, the most suitable transmission window material is germanium or zinc sulphide, since they have wide spectral transmittance that are well characterized.

## 2.10. Camera Calibration and Stability

Most modern, digital, thermoelectric infrared thermal imaging cameras are calibrated by the manufacturer against an NIST standard and usually provided with certificates of calibration. The user may attempt to calibrate or verify the veracity of their thermal imaging device by simply measuring a surface of known emissivity and

temperature and comparing the results.  Overriding the calibration is not usually permitted, since the internal software and calibration information is either proprietary or not disclosed. Despite the fact that infrared thermal imagers are thought of as devices that measure temperature, it is important to realize that all temperature values are estimates based on a mathematical model of the viewing environment and object.

The manufacturer's process of calibration (Minkina and Dudzik, 2009) involves using a blackbody radiation source inside a temperature controlled environment.  The blackbody radiation source is located close to the camera ($\sim$1 m), and $\varepsilon_{\square\square\square\square\square}$ and $\tau_{\text{atmosphere}}$ assumed to be $\sim$1.0.  A calibration curve is then constructed where the sensor signal ($s_i$) is related to a series of different temperatures ($T_i$, K).  Due to the empirical nature of the calibration process, each lens and camera are individually calibrated.  On occasion, calibration information is stored within the file structure and converted using software provided by the manufacturer.  Ideally, the user would have access to the raw signal recorded by the thermal imager to allow for post-acquisition processing of the imaged environment.  Most thermal imaging software performs the calculations for the mathematical model outlined above, allowing the user to alter settings for the background temperature, atmospheric temperature, relative humidity, object emissivity, window transmission, and camera to object distance.

## 2.12. Converting Signal to Temperature

Thermal imaging devices fundamentally translate the electromagnetic radiation within the sensor's range of sensitivity into a temperature-based image, or thermogram. Accurately measuring an object temperature with thermal imaging, however, requires precise knowledge of the radiative environment as well as physical attributes of the object of interest.  Since there are always multiple sources of infrared energy in a thermal image, modern thermal imaging technology makes use of many sources of information to adjust and correct for these contributions. For example, the incident radiative power (*IRP*) detected by the thermal imaging device is actually the sum of the object's emitted radiant power (*ERP*) along with any transmitted and reflected radiant energy (*TRP, RRP*):

$$IRP = ERP + TRP + RRP$$

Typically, it is the ERP that the user sets out to measure, since this can be directly converted to object temperature, following Planck's law and the Stefan-Boltzmann relationship. Ultimately, the thermal imaging sensor measures the entire environment within the field of view, which means that while the image may be focused on a particular region, the entire environment still impinges upon and/or influences the radiation which the sensor detects. The signal arriving at the detector is subsequently modeled though various mathematical algorithms, making certain assumptions. Since the radiation emanating from the object passes through an atmosphere and possibly a transmission window, these additional sources of radiation have to be taken into account (Figure 4). Also, radiation from the atmosphere on the near side and far side of any transmission windows need to be considered as well as any radiation reflected from the transmission window. The entire radiation signal ($s$) detected by the sensor then, can be described as the sum of radiation from the object ($s_{ob}$), the reflective and atmospheric environment between the object and the window ($s_{refl1}$ and $s_{atm1}$), the transmission window ($s_w$), reflection from the transmission window ($s_{reflw}$), and the atmosphere between the window and the camera ($s_{atm2}$) as follows (Minkina and Dudzik, 2009):

$$s = s_{ob} + s_{refl1} + s_{atm1} + s_w + s_{reflw} + s_{atm2}$$

Since we are usually interested in the $s_{ob,}$ by re-arrangement the signal from the object can be formally defined as:

$$s_{ob} = s - s_{refl1} - s_{atm1} - s_w - s_{reflw} - s_{atm2}$$

In cases where there is no transmission window, this simplifies to:

$$s_{ob} = s - s_{refl} - s_{atm}$$

which is why most thermal imaging software typically requires information on the background reflected and atmospheric temperatures before estimating object temperature.

The thermal imaging sensor only detects IR within a specific, narrow band of wavelengths (Figure 1), and thus the precise means of converting incipient radiation to temperature requires an empirical calibration. Manufacturer calibrations involve determining the non-linear $s$ *vs.* $T$ relationship for a technical blackbody using the following modified Planck relationship (Minkina and Dudzik, 2009; Wallin, 1994):

$$s = \frac{R}{e^{B/T} - F}$$

where *R*, *B*, and *F* are empirically fitted coefficients for each lens-camera combination. This empirical fit approximates the integration of the product of blackbody exitance ($M_b$) which is incident on the detector and the spectral sensitivity curve of the camera. In this manner, the signal to which each camera is calibrated can be converted to temperature by simple re-arrangement:

$$T = \frac{B}{\ln(R/S) + F}$$

Although the average user does not need to apply these calculations when using the commercially available analysis software, knowledge of the algorithm used to produce the temperature estimates helps in cases where temperature has already been estimated using default or incorrect settings and a de-convolution of the relationship is required (see supplementary materials for an example). An open-source solution (Package "Thermimage") to assist with these calculations is available for use with the R platform (Tattersall, 2015) and available on the CRAN repository.

## 3. Putting Thermography to Use

### *3.1. Practical Considerations*

A few practical concerns should be considered before embarking in research using thermal imaging. For laboratory data collection of animal surface temperatures, these concerns are typically less important, but for work in the field or in challenging laboratory conditions (*i.e.,* with IR windows), careful mathematical corrections will be required. Things to consider when setting up a scene to capture thermal imaging data are numerous (Holst, 2000), but are typically readily accounted for provided some planning is performed. The user is not typically concerned with atmospheric transmittance, unless the distance and atmospheric humidity are sufficiently high, but before embarking on any field collection of images, a simple, portable weather device should be considered, since all of the pertinent parameters can be collected simultaneously, time stamped, and incorporated into any offline analyses (Greenberg et al., 2012).

In field conditions, attention to convective cooling from wind, especially if there is surface moisture, needs to be given in order to acquire accurate temperature

measurements. Although the typical thermal imaging algorithms will not compensate for convective heat exchange, any convective cooling will still result in lower surface temperatures, and thus, thermal imaging can be used to approximate local differential rates of heat exchange on a body surface.

As thermography is a fundamentally an imaging technique, framing the subject properly follows similar principles to digital photography. Typically the object is centered within the image frame, which allows auto-focus and spot temperature estimation, but also to facilitate offline analysis. Thermal images (especially of objects with heterogeneous emissivities and thermal conductivities) will not necessarily resemble the real life object, and thus centering the object of interest or simultaneous photo-digital images can assist in locating the object of interest during the analysis stage. Some thermal cameras provide simultaneous photo-digital image capture, so that regions of interest on the thermal image can be superimposed on the real object for greater spatial accuracy.

As an imaging technology, thermal imaging cameras can capture an image at any angle of incidence (*i.e.,* measured from the perpendicular to the object), which will not produce an immediately obvious effect. Nevertheless, it is typical for images to be captured at a very low angle of incidence; however, elevated angles will influence the surface emissivity and thus influence the estimated temperature if not accounted properly. Generally speaking, if the angle of incidence is kept less than 30°, then the effects on emissivity are negligible, but above that, emissivity starts to fall precipitously and would need to be measured and corrected during the analysis stage (Holst, 2000).

### 3.2. Overview of Common Errors

It is common for thermal cameras to have a default emissivity setting that may not be that of the object of interest (*e.g.,* 0.92 or 1.0). If only the default emissivity values are used, actual temperature estimates will have systematic errors. For physiological and ecological approaches near average environmental temperatures (15 to 20°C), these errors are typically acceptable, or at the very least, systematic within a given study. Nevertheless, this error can be modeled mathematically prior to any analysis, to assess whether it is acceptable for a study's desired effect size (see supplementary materials). If

the emissivity setting used is higher than surface's true emissivity, then the algorithms will incorrectly assume that some of the incipient radiation in emitted rather than reflected radiation, which will introduce a temperature-dependent error. If the object is warmer than the environment, the object's temperature will be underestimated; conversely, cool objects will be overestimated. If the emissivity is underestimated, a reverse pattern emerges (Figure 5A). For the typical range of emissivities used, this error could be between -2 and +2°C.

Inaccuracy in the reflected background temperature used in the mathematical algorithms will introduce error that depends on the magnitude of the object's reflectance (1-$\varepsilon$), as well as the reflected temperature used. If the reflected temperature is overestimated, this attributes too much of the incipient radiation to the reflected environment and thus underestimates object temperature; the reverse is true for underestimating the reflected temperature (Figure 5B).

A default relative humidity of 50% is typical in much thermal imaging algorithms, which is appropriate for many indoor applications. If the object is at longer distances away from the camera, there would be sufficient transmission loss through the atmosphere, which would depend on the amount of water vapour as well as the object temperature. If relative humidity were overestimated, a positive error would result if the object was warm, but a negative error would result if the object was colder than the environment; the reverse would be true for an underestimation in relative humidity (Figure 5C). Usually, these effects are minor for short distances (<10m) but could lead to values that are -2 to +2°C different from the true temperature.

A final practical consideration when setting up for thermal imaging is whether to include a IR transparent window (see section 2.9). When analyzing thermal images captured behind a window, temperature estimates are much more sensitive to all of the parameters used in the mathematical algorithms. Similarly to above, mis-estimating transmission will produce complex errors in estimated temperature that are dependent on the object's emissivity as well as the reflected environment's temperatures. In a simplified situation, however, overestimating the actual transmission levels will overestimate object temperature if background is higher than the object temperature, and underestimate object temperature if background is lower than the object temperature.

Opposite patterns occur when underestimating IR window transmission (Figure 5D). Typical errors in estimated temperature for minor errors in transmission might range from -2 to +2°C, however IR windows that are sometimes used in comparative physiology (Dzialowski et al., 2014; Palmer et al., 2004; Tattersall and Milsom, 2003) often have much lower transmission levels ($\tau$=0.5 to 0.7), and the error estimates could be much greater, unless an empirical calibration is performed, or only relative changes are required.

### 3.3. Ensuring Quality Thermal Imagery

Numerous challenges exist to obtaining focused, and therefore, accurate thermographic data on living systems. For example, reliance on auto-focus on fast moving objects, or under conditions of elevated solar radiation when object-background contrast is low will invariably produce blurry images or thermal "ghosts" due to the low response rate of microbolometers. Proper focus achievement may seem trivial, but with respect to thermal imaging, it is more than simply an aesthetic convenience. First, an image out of focus lacks the spatial resolution to detect small scale differences in temperature. Second, there may be automatic distance detection in software packages, which would lead to inaccurate assumptions about atmospheric transmission, since focus distance incorrectly reflects actual distance. Finally, the more important challenge with out of focus thermal images is due to a "background blending" effect, which will influence the estimated object temperature. When an image is not in proper focus, the low spatial resolution essentially averages out a complex array of different temperatures across a wider range of pixels. If the background temperature is much cooler than the object of interest, then the object temperature will be underestimated due to this blending effect. A similar effect would happen with a warm background and cool object temperature, except that object temperature would be overestimated. Small errors in focus distance can produce large errors in estimated temperature (Figure 6). For an object-background temperature difference of ~20°C, the error can be as high as -5°C, whereas for object-background temperatures differences of 50 to 70°C, the error can be as great as -40 to -50°C. This author recommends that publications using thermography provide their raw data or sample thermal images, and to be cautious with images taken on

rapidly moving objects which are difficult to achieve proper focus, especially if the background temperatures are >20°C different from the object of interest.

When performing IRT in the field, the user has little to no control over the environmental parameters, however in a more controlled situation, such as in the laboratory, especially when working with ectothermic animals whose body temperatures are very close to ambient temperature, the user can enhance image contrast by altering the properties of the background. If a surface with low emissivity (*e.g.,* aluminum foil tape) is placed underneath an ectotherm (whose actual temperature will be similar to background temperature), the animal will show an apparent contrast with the background and be more readily detected. This approach may help with detecting moving animals as well, although the highly reflective surface will also reflect room temperature radiation, and so the foil surface should be avoided for any determinants of surface temperature.

When working in the laboratory, it may be critical to have a thermal imaging video designed to capture a transient event or a time lapsed rendering of a change in temperature over time. When examining small changes in temperature, however, drift is an important consideration. Although many thermal imaging systems can detect temperature differences less than 0.05°C, building HVAC systems only regulate room temperature to ±0.5°C, which means that time based IRT is prone to disturbance from externalities that are often difficult to control (*e.g.,* uneven air flow, room temperature control beyond tolerance limits). Another temporal inconsistency in thermal imaging is electronic noise and drift from the instrument (Figure 7). Modern microbolometers (the more commonly used sensor in LWIR cameras) are actually an array of thousands of temperature sensors, each of which is subject to random (*i.e.,* Gaussian) changes in sensitivity. Over time, then, each individual pixel will produce a different response, and drift in its response unless it is "corrected" to the mean pixel response to correct for sensory non-uniformity. Most research-grade thermal cameras have a built-in non-uniform correction (NUC) function, which operates periodically, resulting in a shutter being placed in front of the array for ~1 s. Although the NUC feature interrupts the video feed, it allows for each pixel to be exposed to a constant thermal source and calibrated to the mean pixel sensitivity such the random noise that increases drift and inter-pixel variability is minimized. Failure to use the NUC feature will also produce images that

appear "grainier" in composition due to the random pixel-by-pixel variation in response sensitivities. Similarly, thermal imaging cameras should be allowed a period to "warm-up" in order to allow the self-calibration for non-uniformity to commence and the electronics to reach a stable temperature. This self-calibration is separate from the manufacturer's calibration that provides the curve fitting procedures for blackbody radiation. The manufactures do advise that thermal imaging cameras are sent for yearly calibrations, although the need for this can be verified by assessing the temperature of an object of known temperature and emissivity; distilled water ($\varepsilon$=0.95) heated to a known temperature is a simple way to verify camera calibration.

### 3.4. *Minimum Spatial Resolution*

Thermal imaging systems typically provide instantaneous field of view (IFOV) values, also called their spatial resolution, which allows one to assess the minimum resolvable size of object that can be detected by a single pixel. The IFOV is the angle over which the detector senses radiation, which means that one can calculate the minimum measurement spot size (*MSS*) detectable by the camera as:

$$MSS = d \times \theta_{IFOV}$$

where $d$ is the distance (m) from the target to the camera, and $\theta_{IFOV}$ is the IFOV in radians. For example, if you were imaging an animal that was in total 10 cm high, and the $\theta_{IFOV}$ was 0.00065 radians, the maximum distance you could reliably resolve the animal would be 153 m. This value, however, only represents the size of one pixel. Depending on the research question, a more realistic measurement spot size might be 50 pixels in height, which would provide plenty of resolving capacity of an animal, but would require the image to be obtained at only 3 meters in distance. Applying this information prior to making measurements is essential for those planning on purchasing thermal imaging devices, since many of the inexpensive alternatives available are unlikely to provide the necessary spatial resolution required for research quality data collection; by extension, authors are encouraged to provide this information in research studies to better inform on the reliability of distant temperature estimates. In addition to minimum spot-size detection, the spatial resolution has implications for accurate estimates of temperature with IRT that depend on distance and sensor resolution (Faye et

al., 2016). In a recent study estimating distance influences on IRT estimates of thermal mosaic, Faye et al. (2016) discovered that images captured from longer distances (>20 m) invariably underestimated surface temperatures by as much as 3°C, an effect that is a complex relationship involving atmospheric conditions, pixel size, and how solar radiation interacts with complex structures. Whenever possible, objects of interest should occupy a sizable number of pixels in the final thermal image, and distance effects on temperature estimates should be empirically assessed, and at minimum, modeled mathematically.

## 3.5. *Thermal Image Analysis and Software*

Analysing thermal images, especially videos from conscious and active animals is a laborious process. Unlike many of the applications for which IRT was developed (physics, engineering), animals are rarely stationary with respect to the captured image frame, so any time-based analyses are plagued with changes in shape, perspective, and distance, and existing thermographic software packages appear to lack automation features that include object tracking along with temperature analysis. To date, the author is not aware of software packages that incorporate thermal analysis with motion sensing or object tracking, although customized solutions could be achieved with sufficient computation skills and access to existing analytical platforms (Abramoff et al., 2004; MATLAB, 2015). Typically, users are required to draw a region of interest (ROI) over the surface they wish to examine and simple mean, minimum, maximum and standard deviation of the pixels within the ROI is possible. The most powerful programs allow for ROI data to be examined over time. With respect to physiological data, movement artifacts typically make these impossible to use. One of the limiting factors in infrared thermal imaging is the file format. Image files are not always saved in a publically accessible format and require commercial software for analysis. Although normally provided at the time of purchase, unless the user has computer programming skills, they are at the whim of the company supplying the software. Open source alternatives to these commercial software packages are not available at present (Minkina and Dudzik, 2009), however, customized approaches could be employed (see supplementary materialTattersall, 2015).

## *3.6. Thermal Image Presentation*

There are two approaches to thermal image presentation, one which emphasises or accentuates small differences in temperature and the other which produces a colour images that follow a more gradual, linear contrasting scale. In the former case, colour palettes that exhibit high contrast (*e.g.,* rainbow palette) enhance the visualisation of small temperatures difference; these are often used in medical or biomedical imaging. In the latter case, colour palettes like FLIR's iron palette (used throughout this review) create a more monotonic contrast (from black through blue, magenta, orange, yellow to bright white) while still producing a colourised image; these images also appear more natural looking, although still different from how photo-digital images would appear. Computationally, concerns about palette use are not important if working with radiometric images, since these files also encode the raw sensor data for each pixel in a proprietary file format at 12 to 16 bits of resolution, while the image is simply the means to present the results. Nevertheless, not all users of thermal imaging devices have access to radiometric images, and thus the nature of file saving for certain low-end, consumer-oriented thermal imagers will present limitations to analysis. For example, the maximal thermal image resolution of a radiometric image is equivalent to the sensor sensitivity range divided by the number of bits of information (e.g. $140°C / 2^{16} = 0.002°C$). For comparison, a non-radiometric image saved with at a typical maximum – minimum temperature difference of 20°C would have a much lower (40 times) resolvable temperature difference (e.g., $20°C / 256 = 0.08°C$). Furthermore, if the user only has access to a non-radiometric image file, a look up table of the false colour gradient of temperatures with corresponding RGB values will need to be used and calibrated appropriately. More sophisticated analysis of the non-radiometric images, requiring consideration of emissivity, transmission and environmental variables would be difficult to achieve.

## 4. Thermal Imaging in Comparative Physiology

The uses of any imaging technology are limited primarily by the resourcefulness of the user. Provided the constraints and limits to thermal imaging are considered and accounted for, any change in surface temperature can be measured and incorporated with

simultaneous physiological or behavioural measurements, providing insights into physiological processes. Below, I highlight a number of applications of IRT in the field of physiology and zoology, and conclude with a theoretical explanation of the association between surface temperature changes and underlying heat flow to assist in better modeling and analyzing of thermal imaging data in order to facilitate new or enhanced comparative physiological insights, particularly those into peripheral cardiovascular regulation.

## *4.1. Non-Contact Thermometer & Thermal Preference*

The most straightforward use of the thermal camera is for measuring surface temperature of animals, usually with the objective to infer or estimate core body temperatures. For large animals, surface temperatures will not be equivalent to body core for simple reasons of thermal inertia, as well as the greater potential for peripheral vasomotor control with larger body size (Mortola, 2013; Phillips and Heath, 1995). Generally speaking, if core body temperature is needed, IRT cannot provide this information, except for the study of small ectothermic organisms. Khan et al. (2010) used IRT to estimate body temperatures of small lizards (body mass <3g), finding high correlation ($r^2$>0.95) between skin surface temperature and core body temperature. This approach enabled the continuous assessment of body temperature preference as well as the influence of aggregation and social interactions on thermoregulation (Figure 8). This approach would be virtually impossible to perform on instrumented animals (Khan et al., 2010).

IRT can also capture thermal information on thermal inertia in ectotherms. Pincebourde et al. (2009) discovered that intertidal sea stars alter their total body water content in a manner that enhances thermal inertia under times of low-tide heat stress; when submerged during high tide, they accumulate more water and thus change temperature more slowly when exposed to air at low tide. Investigations of the body surface temperatures of 18 species of lizards has also revealed that the differential between surface temperature and ambient temperature was greater in the larger lizards (Garrick, 2008). The mode of behavioural thermoregulation influenced the strength of this differential; heliothermic lizards (those that bask to warm) demonstrated a positive

relationship, exhibiting greater thermal inertia with larger body size, while thigmothermic lizards (those that primarily derive heat from the substrate) showed a negative or no relationship with body size, although the small sample size of species suggests caution with this interpretation. One interpretation of these data is that heliothermic lizards have enhanced control over cardiovascular regulation of blood flow, which would enhance their capacity to retain body heat from basking.

Thermoregulatory behaviour of reptiles is also readily assessed with IRT, providing insights into thermal preference and body temperature set-points (Blumberg et al., 2002; Tosini and Avery, 1993; Tosini and Avery, 1994; Tosini et al., 1995). For example, Blumberg et al. (2002) studied thermoregulatory shuttling behaviour in neonatal Madagascar geckos to examine whether incubation temperatures had long-term impacts on thermoregulatory set-points. Using IRT, they captured thermal images and videos allowing for the surface temperature of the skin to be assessed at the point in time when the lizard made a behavioural decision to shuttle from a hot environmental to a cold environment, as well as the reverse. IRT, therefore, served as a non-invasive approach to obtaining the upper and lower avoidance temperatures, which would be a metric for thermal preference. Interestingly, the incubation temperatures were found to impact thermal preference; high incubation temperatures lead to higher thermal preferences in geckos, suggesting incubation-based plasticity in thermoregulatory behaviour (Blumberg et al., 2002).

IRT is typically used to infer information on non-instrumented animals and one application is on those engaged in semi-normal behaviours, such as flight (Lancaster et al., 1997; Powers et al., 2015; Ward et al., 1999). The value of IRT in these applications is to assist in finding the sites on the body of highest surface temperatures, rather than for core temperature estimation or thermal preference. In bats, for example, wing temperatures during flight remain constant and quite close to ambient temperature, even though body temperature rises during the initial stages of flight. The bat wing, by virtue of its large surface area, contributes strongly to overall heat exchange during flight, even though its surface temperature does not change much during flight. Similarly, although at a much larger scale, Betke et al. (2008) used IRT to monitor flight behaviour of whole colonies of Brazilian free-tailed bats, discovering emergence flights occurred at

population-specific rhythms, as well as using IRT to enhance accuracy of other census techniques. Although not used in a physiological context, IRT has been used in combination with other imaging techniques for detecting novel nests and burrows and providing census estimates of non-flying mammals in the field (Boonstra et al., 1994). Boonstra et al. (1994) were successful in detecting free-ranging mammals (squirrels, hares, jumping mice) as well as determining burrow use, although IRT was not effective for detecting species with well insulated burrows. Subsequently, Boonstra et al. (1995) employed IRT for detecting birds in the wild, but met with mixed success. Although IRT will detect endothermic animals, the goal of some field research may be to discover novel nests or nighttime roosting sites that would be undetectable through simpler techniques (*i.e.*, ones that would not be obvious in the visible spectrum). Boonstra et al. (1995) also offered a number of insightful caveats to the using IRT in the field: the signal (temperature differential) is often too weak during the warmest parts of the day, objects in the field that can absorb significant solar radiation cause interference and many false positives, insulating properties of nests prevent heat transfer and thus evade detection, and, finally, the generally high expense of IRT precludes its utility for many field researchers. Personal experience has also shown that IRT is limited in this regard, especially due to the fact that many objects show different rates of heat exchange in the environment, and most especially because environments with significant vegetation cover produce interference that IRT cannot easily overcome.

## *4.2. Assessing Evaporative Cooling*

Since IRT measures surface temperature, phenomena that alter heat exchange to the surface can be assessed. One of the most readily assessed phenomena is evaporative cooling. On any moisture surface, liquid water is spontaneously converted to water vapour at a rate inversely dependent on the water vapour pressure. As evaporation is an endergonic process, requiring the input of energy equivalent to the latent heat of vapourization of water, moist surfaces (*e.g.,* epithelial lined upper airways, thin-skinned animals) in contact with low humidity environments will demonstrate cooling (Figure 9). Since thermal conductance of the air is very low compared to tissues, vapourisation will remove heat from the most permissive source, which is usually the animal's tissue. Any

additional air flow that disrupts surface boundary layers will facilitate even greater evaporation, causing convective forcing and even greater cooling (Figure 10). The potential for evaporative cooling playing an important role in thermal physiology is well known (Gates, 2003), although recent work with IRT has uncovered interesting behavioural and physiological interactions. Both Borrell et al. (2005) and Tattersall et al. (2006a) noted the potentially powerful effects of evaporation on whole head cooling in many reptiles. Tattersall et al. (2006a) reviewed the prevalence of respiratory cooling in reptiles using IRT, and noted that the degree of respiratory cooling in terrestrial lizards, turtles, snakes, and caiman is typically more profound at higher ambient temperatures and at lower humidity. This whole rostrum cooling is associated with a more precise control over head and brain temperature in reptiles (Tattersall et al., 2006a). Reptiles are especially prone to prolonged cooling of the head and rostrum because their breathing pattern is one in which exhalation precedes inhalation, followed typically by a non-ventilatory period (Tattersall et al., 2006a). These non-ventilatory pauses after inhalation maximize the potential cooling effect since the airways do not receive warmer lung air until the start of the next breath; while the airways remain cool during the ventilatory pause, the rostrum equilibrates with the cooler airways through conduction. Respiratory cooling forces the rostrum surface to be as great as 5°C cooler than other body surfaces, which enhances thermal detection and prey capture in pit vipers due to the close proximity of the pit organs to the upper airways (Cadena et al., 2013). Indeed, at first hand, it appears that pit organ cooling via respiratory evaporation functions analogously to the early models of thermal imaging devices that required cooling in order to reduce background radiation and enhance thermal stability of the sensor. More specifically, the respiratory cooling probably acts to reduce thermal "after-images" and enhance detection of a moving object's temperature, essential to heat detecting predators like rattlesnakes. IRT was critical to this discovery because it measures temperatures non-invasively and allows for normal behaviours to occur unimpeded by instrumentation.

### 4.3. Assessing Tissue Freezing and Insect Cold Tolerance

Just as surface evaporation leading to phase changes in water which cools the surface, at the other end of the physical scale, water can be observed to freeze with IRT due to the heat of fusion of water that is released upon the phase transition of water to ice. Many insects, and some ectothermic vertebrates tolerate body freezing during the winter (freeze tolerant), while others are sensitive to body freezing (freeze avoidant). Remarkably, until recently (Gallegoa et al., 2016) IRT appears not to have been extensively used in cold tolerance studies in animal physiology, although it has been examined in studies of plant tissue freezing (Wisniewski et al., 1997). Nevertheless, IRT can be useful in recording the heat of fusion of water as tissues freeze (Gallegoa et al., 2016; Skandalis et al., 2011). This approach allows for a rapid, non-invasive means to assess the minimum supercooling point in insects, which is often used as a metric for cold tolerance in freeze-avoidant insects (Figure 11). By not instrumenting the insects with external temperature probes, they are also able to behave freely (Palmer et al., 2004) during the measurements, allowing for simultaneous behavioural assessments. Another advantage to using thermal imaging for studying freezing events is the potential for examining where the ice-front originates in the body. Since ice nucleation in supercooled liquids is spontaneous, freeze-avoidant insects typically remove ice nucleators in order to promote tissue supercooling (Tattersall et al., 2012). If tissue freezing occurs in a particular tissue, it would allow for more mechanistic interpretations of freezing risk factors (Skandalis et al., 2011). In freeze tolerant animals, IRT would also allow for repeated measurements of freeze-thaw cycles over the course of the winter. One technical challenge with using thermography at low temperatures is an inevitable accumulation of ice crystals from room humidity which can not only impede visualization, but also act as external nucleation sites if they come in contact with the specimen.

### 4.4. Assessing Thermogenesis and Brown Adipose Tissue Activation

Understanding mammalian energetics and the control of thermogenesis has long been a focus of comparative biomedical models as well as basic hibernation (Bouma et al., 2012). IRT has contributed some answers in this regard, despite the fact that

measuring the heat produced from a specific tissue, such as brown adipose tissue (BAT), using IRT is a challenge due to overlying insulation, tissue depth, as well as the fact that blood flow may be increased at the same time as thermogenesis is induced. One situation where thermogenesis can be readily observed, however, is during arousal from torpor in hibernating mammals. During torpor, when body temperature has fallen close to ambient, there is a profound vasoconstriction with most of the blood pooling in the core, and only the brain and heart show evidence of being warmer than the surroundings (Florant and Heller, 1977; Heller and Hammel, 1971, 1972). Indeed, during hibernation, the periphery is still colder than the core, due to a strong sympathetic drive that is only released later during arousal from torpor (Osborne et al., 2005). IRT is able to track the arousal process from hibernation (Phillips and Heath, 2004); since hibernating mammals remain almost stationary when in torpor and during arousal, video thermography is able to record the entire arousal process, from body temperatures ~0°C up to euthermic levels (~38°C). Indeed, IRT allowed Phillips and Heath (2004) to uncover that the smaller 13-lined ground squirrels, compared to the larger marmots, perfuse the distal regions of the body during arousal without compromising warming of the deep body temperatures. Nevertheless, a common pattern during arousal from torpor is for the heat produced in the BAT to be retained in the anterior region (head and thorax), a pattern which is readily observed with IRT.

If IRT could be shown to be capable of quantitatively measuring BAT activation, then it might be able to replace the current method whereby whole body metabolism is measured following norepinephrine injection. The simplicity of IRT is appealing, since in rodents, the primary BAT is located in the interscapular region, conveniently located in the upper dorsal region and easy to capture with imaging provided the dorsal fur is depilated (Figure 12). Jackson et al. (2001) studied this in the short-tailed field vole, but found that the skin surface over top of the BAT could not be correlated to the metabolic increment that accompanies norepinephrine injection, suggesting a rather poor ability of IRT to detect thermogenesis within the BAT. However, in this study, the animals appeared to have been handled during the IRT measurements of skin temperatures, which were not measured simultaneously with oxygen consumption. Handling can lead to emotional hyperthermia via altered peripheral blood flow and thermal conductance

(Cabanac and Gosselin, 1993; Michel et al., 2003; Thompson et al., 2003), which could explain the low correlation between heat production and BAT skin temperature.

In contrast to Jackson et al. (2001), numerous studies have still utilized IRT to visualize BAT activation (Blumberg et al., 1999; Blumberg et al., 1992; Hodges et al., 2008). For example, Hodges et al. (2008) demonstrated that IRT measures of skin surface temperature over the BAT of mice rose similarly to internally measured BAT temperatures, supporting the potential for surface temperature estimates of BAT activation. In neonatal mammals, where fur does not interfere and other thermogenic mechanisms may be underdeveloped, IRT is quite effective at detecting BAT thermogenesis. Using IRT, Blumberg et al. (1999) showed that leptin is involved in the disinhibition of BAT thermogenesis in neonatal mammals, demonstrating its role in energy homeostasis. Similarly, using knock-out mice deficient in serotonin producing neurons, Hodges et al. (2008) demonstrated with IRT that serotonin is required to activate pre-sympathetic neurons innervating brown adipose tissue.

In contrast to endotherms, assessing thermogenesis with IRT in ectotherms is simpler due to the lack of external insulation. What little insulation certain ectotherms possess is insufficient to retain internally produced heat. Most studies of thermogenesis in ectotherms have focused on hymenoptera (Stabentheiner et al., 2012; Stabentheiner and Schmaranzer, 1987), primarily due to their size and highly active lifestyle, but also due to the ease of imaging. In insects, thermogenesis is primarily muscle-based and is localized to the thorax. In honeybees and bumblebees, this thermogenesis is used to maintain elevated thorax temperature at low temperatures to facilitate active foraging in the cold (Dzialowski et al., 2014; Kovac et al., 2007), but has also been linked to food quality (Mapalad et al., 2008). The thermogenesis is also highly sensitive to changes in oxygen levels, suggesting that it is strongly based on aerobic metabolism (Dzialowski et al., 2014; VanNerum and Buelens, 1997). Interestingly, IRT has also revealed that some degree of thermogenesis is present in bees at rest, even at elevated temperatures, suggesting that not all of the thermogenesis serves a role in thermoregulation (Dzialowski et al., 2014; Kovac et al., 2007). IRT has also shown that under certain conditions, thoracic heat production is retained within the thorax, whereas at elevated temperatures and during flight, this heat is distributed to the abdomen and head to prevent overheating

(Verdu et al., 2012). Not all thermogenesis in ectotherms, however, is muscular based. For example, in snakes, IRT has revealed a whole body thermogenesis that accompanies the processes of digestion. This specific dynamic action of feeding leads to metabolic rates that last for days that are up to 10 times above resting levels (Stuginski et al., 2011; Tattersall et al., 2004), which leads to body temperatures in normally ectothermic animals reaching up to 2°C higher than ambient temperatures.

## 4.5. *Assessing or Estimating Insulation from Surface Temperatures*

Since IRT provides a measurement of surface temperatures, it is possible to achieve an instantaneous assessment of the insulating covering of an endotherm (namely, fur and feathers). Although this assessment will primarily be diagnostic rather than quantitative, comparisons of surface temperatures under identical conditions follow the principles of thermal conduction across an object in steady state:

$$\dot{K} = \frac{kA}{x} \cdot (\Delta T)$$

where $\dot{K}$ is the rate of heat transfer (Watts), $k$ is the thermal conductivity of the pelage (dependent on pelage density), $A$ is surface area, $x$ is pelage thickness, and $\Delta T$ the gradient of temperature across the pelage (usually $T_{skin} - T_{surface}$). To demonstrate how insulation impacts thermal imaging (Figure 13), this relationship can be re-arranged to the following:

$$\Delta T = \frac{\dot{K}}{k} \cdot \frac{x}{A}$$

which reveals a number of simple predictions. The first is that $T_{surface}$ will only ever approach $T_{skin,}$ for an endotherm in steady state, since heat will usually be flowing from the animal to the environment. From this relationship, it is also evident that the temperature gradient across the insulating layer is inversely proportional to the insulator's thermal conductivity ($k$). Thus, an animal with very dense pelage that traps more still air should exhibit cooler fur temperatures due to the larger $\Delta T$ across the insulating layer. Likewise, this relationship also predicts a smaller $\Delta T$ for endotherms with fat insulation compared to those with fur or feather insulation, since $k$ is approximately 5 times higher for fat and blubber compared to fur and feathers (Dawson et al., 1999; Dunkin et al.,

2005). Furthermore, if $x$ is lowered, the $T_{\text{surface}}$ will be higher, all else being the same (Figure 13); likewise, thicker insulation as viewed through a thermal camera will present with a lower surface temperature than thin insulation. This effect can be easily demonstrated in domesticated animals that are reared for wool and fibre; prior to shearing fibre, surface temperatures of the llama's normal 15 cm thick pelage was ~26°C, compared to surface temperatures of ~33°C when the fibre was clipped to 1 cm thick (Gerken, 1997).

One comparative study of two mole-rat species under similar conditions analysed surface fur temperatures in order to detect regions of differential heat loss. Lower surface fur temperatures of the solitary species suggested a denser and longer fur throughout its body compared to the social species of mole-rat (Sumbera et al., 2007). These authors were also able to conclude that the solitary species with denser fur had trouble dissipating heat at higher temperatures, which has implications for core temperature maintenance when burrowing at high temperatures. In this example, insulation capacity itself was not formally measured, although IRT allowed for predictions about thermoregulatory capacity to be made. What IRT cannot provide is an absolute measurement of thermal conductance (*i.e.*, $kA$) since local heat flux ($\dot{K}$) needs to be known (typically measured by a heat flux sensor or calorimeter). Since changes in insulation thickness ($x$) predict different rates of heat by conduction, using $T_{\text{surface}}$ (and indirectly inferring $\Delta$T assuming a constant $T_{\text{skin}}$) obtained from IRT is overly simplistic and only likely to work in experimental situations where all other parameters can be controlled (*cf.* Kvadsheim et al., 1994).

## 4.6. Whole Body Heat Exchange in Endotherms

One hopeful promise of IRT is the potential for non-invasive measurements of energy requirements in animals in the wild. In principle, this is possible, but relies on the incorporation of many simplifying assumptions. The first assumption is that of steady state. For an endothermic homeotherm, steady state production of heat balances out heat exchange with the environment, resulting in constant body temperature. A comprehensive treatment on the subject of steady state heat exchange is beyond the scope of this review, since more than thermography is required for the estimations, however,

numerous published studies provide the necessary biophysical background to use surface temperatures to model heat exchange (Blaxter, 1989; Gates, 2003; Monteith and Mount, 1974). In principle, the approach to assessing total heat loss ($Q_{tot}$) involves using the IRT estimates of surface temperature to calculate each major body surface's regional heat loss and summing all of these to determine total heat loss. Usually, radiative ($Q_r$) and convective ($Q_c$) heat loss are determined for each surface (conductive heat loss is often ignored if the contact surface with the ground is negligible) according to:

$$Q_r = \varepsilon \sigma A (T_s^4 - T_a^4)$$
$$Q_c = h_c A (T_s - T_a)$$

where $\varepsilon$ is the emissivity, $\sigma$ is the Stefan-Boltzmann constant, $A$ is the surface area (m$^2$) of the body part in question, $T_s$ is the surface temperature of each specific body region, $T_a$ is ambient temperature (°K) and $h_c$ is the heat transfer coefficient for the region, which can be determined from the following relationship:

$$h_c = \frac{Nu \cdot k}{D}$$

where $k$ is the thermal conductivity of air at a particular $T_a$, $D$ is a characteristic dimension for the surface, and $Nu$ is the Nusselt number for each particular body surface. The $Nu$ value in turn depends on the Reynold's number. Since the Reynold's number depends on object size and air velocity, there is no singular value for $h_c$ for the entire body, although typically smaller regions (*e.g.,* appendages) have larger $h_c$ values. All of these terms require that the animal be modeled as a series of simplifying geometric shapes, and thus even when accurate dimensions are available, the entire model may miss nuanced differences in shape that are not fully captured with an additive model. In animals, these estimates have rarely been confirmed for their predictive ability since simultaneous measurements of metabolic heat production are rarely conducted. Nevertheless, one of the most comprehensive approaches to predicting heat loss was a comparative study of three ratites (Phillips and Sanborn, 1994), similar to that outlined above. Their estimated rates of heat loss were compared to previously published resting heat production levels and generally were within ±15-30% of previous estimates of energy expenditure in each of the species examined. Prior to IRT approaches, simple hand-held thermometers were used in combination with indirect calorimetry, confirming

that heat balance estimates from surface temperatures show strong association with metabolic heat production (Maloney and Dawson, 1994). These estimates may be reasonably close considering the various assumptions, but are still only estimates obtained from animals at rest. Other studies using IRT to estimate sensible heat loss have focused on cold-dwelling animals. Munn et al. (2009) elucidated through IRT that although juvenile Muskoxen lost heat more readily (per $m^2$ surface area) than adults, heat losses in both adult and juveniles consisted of 2-6% of their estimated daily digestible energy intake, rates that were minimized through peripheral heterothermy and exceptionally efficient insulation. McCafferty et al. (2013) modeled heat exchange in emperor penguins using IRT and found that due to radiative exchange with sky temperatures that were much lower than air temperature, certain parts of the body surface were actually cooler than air temperature, leading to the intriguing conclusion that these surfaces could gain heat via convection from air temperatures warmer than the bird's surface. Applying the estimates appear reasonable under conditions of low solar radiation, however, under full sun conditions, significant short-wave reflection is likely to occur and would need to be accounted as a source of heat gain (McCafferty, 2007; McCafferty et al., 2013); this necessarily requires estimates of short-wave reflectance as well as solar radiative flux, and so heat flux estimates from IRT performed in full sunlight should be considered with caution.

## 4.7. Thermal Windows in Endotherms

As endotherms, balancing body heat requires regulation of metabolic heat production as well as regulation of blood flow, especially to peripheral regions of the body. The core-shell model of thermoregulation has often been used to describe how homeothermic endotherms maintain a relatively constant core temperature (Jessen, 2001). In this model, the core, where body heat is generated, is held at a constant temperature, while the shell is free to vary in temperature. These changes in temperature are effected primarily by changes in peripheral blood flow. Greater peripheral blood flow usually leads to greater peripheral heat loss to the external environment. Furthermore, by diverting warmer core blood to the periphery, endotherms are able to raise the temperature of their superficial organs and appendages. The higher temperature of the

body's surface is what provides the driving force for heat loss to the environment.
Overall, this model allows for heat conservation at low ambient temperatures because the
gradient for heat loss to the environment is reduced.  At intermediate temperatures, slight
alterations in peripheral blood flow are predicted to occur as endotherms adopt
metabolically inexpensive means of thermal adjustments within their thermoneutral zone.
Indeed, surface temperature estimates of peripheral tissues like the feet and tails of
rodents have been used to estimate thermoneutral zones of small mammals (Romanovsky
et al., 2002; Rudaya et al., 2005) since the ambient temperatures at which tail surface
temperatures are most variable also coincide with the animal's thermoneutral zone and
preferred temperatures (Almeida et al., 2006; Rudaya et al., 2005).  The advantage of
using IRT with voluntary thermal choice is that evidence for vasodilation of peripheral
structures can be used to imply changes in the thermoregulatory set-points.
Lipopolysaccaride injection in mice mimics fever, which causes them to show an
elevated thermal preference as well as a rise in the threshold ambient temperatures at
which tail vasodilation occurred (Rudaya et al., 2005).

To date, "thermal windows" of body surfaces with elevated and/or variable heat
exchange have been described in various animals, including hare, rabbit and elephant ears
(Hill et al., 1980; Hill and Veghte, 1976; Mohler and Heath, 1988; Phillips and Heath,
1992), guanaco fur (Morrison, 1966), penguin feet (Wilson et al., 1998), bird bills (Hagan
and Heath, 1980; Tattersall et al., 2009), digits (Moritz and Dominy, 2012), combs and
wattles of numerous fowl (Buchholz, 1996), ungulate horns and antlers (Picard et al.,
1994; Taylor, 1966), and patches of skin in seals and elephant seals when hauling out on
land and engaging in physical activity (Mauck et al., 2003; Norris et al., 2010).  In
contrast to well insulated areas of the body, these regions typically have quantitative and
qualitative differences in vasculature (Midtgard, 1980, 1984; Villarreal et al., 2007).  The
density of anastomoses shunting arterial blood to the venous system are generally higher
in these regions of the body.  For this reason, these surface have been referred to as
"thermal windows", inasmuch that they can be opened or closed sites for heat exchange
from the animal to the environment.

Another important feature of thermal windows is that they be under normal
thermoregulatory control.  IRT analysis has demonstrated this in the ear pinna, face, and

feet temperatures of rabbits and foxes, which respond to thermal stimulation of the pre-optic area of the anterior hypothalamus (Klir and Heath, 1994; Mohler and Heath, 1988); vasodilation of the ear pinna occurs when the hypothalamus was heated and vasoconstriction when the hypothalamus was cooled. In some cases, however, the heat emanating from thermal windows is simply a by-product of a sensory process, such as seen in the middle digit of the aye-aye that warms up during active use and flexion, whereas in other cases these sites may help to drive greater evaporative cooling from the surface in marine mammals that are challenged with staying cool when on land (Mauck et al., 2003). In some cases, the capacity for heat loss from thermal windows has been calculated; in elephants, vasodilation combined with flapping of the ears can promote the loss of heat up to the equivalent of 100% of resting metabolic heat production (RHP). Bird bills, on the other hand, without the need for augmented movement have been estimated to be capable of losing 9.2 to 84% of RHP in pekin ducks (Hagan and Heath, 1980) and up to 480% of RHP in toco toucans (Tattersall et al., 2009). These estimated rates of heat loss are substantial but refer only to transient rates of heat transfer from mathematical models of heat exchange. In order to assess the feasibility of these estimates of heat exchange, it is reasonable to ask what portion of cardiac output would be required to perfuse the organ. In the extreme case of the toucan bill, Tattersall et al. (2009), estimated the maximum rates of heat loss from the bill to the environment to be as high as ~10 Watts at an ambient temperature of 20°C, whereas resting whole body heat production has been estimated to be ~3 Watts (McNab, 2001). To calculate the portion of cardiac output required to enable this, a number of assumptions can be made. First, the blood entering the bill is at body temperature ($T_b$ ~40°C) while the blood leaving the bill is equal to the ambient temperature ($T_a$ ~ 20°C), which is unlikely but would represent the maximum estimate of heat transfer from blood. The heat transferred by the blood can be determined as follows:

$$Q = (T_b - T_a) \cdot c_b = (40 - 20) \cdot 4187 = 83.7 \text{ J}$$

where $Q$ is total heat in Joules, $T_b$ is 40°C, $T_a$=20°C, and $c_b$ = specific heat capacity of blood = 4187 J/kg/°C, which is equivalent to 83.7 J/cm$^3$ of blood. Next, the blood flow necessary to dissipate 10 W (=10 J/s) can then be estimated as the rate of heat loss divided by the quantity of heat carried by the blood, which is 10 J/s divided by 83.74

35

J/cm$^3$ = 0.11 cm$^3$/s.  If one assumes that blood releases 4 cm$^3$ O$_2$/100 cm$^3$ blood (*e.g.,* the (A-V)$_{O2}$ to fuel resting metabolism), and the oxycaloric equivalent ($CE_{O2}$) is 1 cm$^3$ O$_2$/20.9 J heat, the required cardiac output to fuel resting heat production can be estimated by a re-arrangement of the Fick Equation:

$$CO = \frac{RHP \cdot CE_{O2}}{(A - V)_{O2}}$$

which leads to an estimated *CO* of 3.58 cm$^3$ blood/s which is far higher than the 0.11 cm$^3$ blood/s estimated for blood flow to the thermal window.  Indeed, the proportion of total cardiac output to the thermal window would be estimated to be 0.11/3.58 = 3%.  Rather than a 20°C drop in blood temperature, a more conservative value of 5°C would predict heat content to be 4 times higher, which translates into the thermal window requiring 12% of resting cardiac output.  Even this comparatively high value could be easily accommodated, since the cardiovascular scope for change in most endotherms is ~5-10 times that at rest (Hillman and Hedrick, 2015).

## *4.8. Modeling Surface Temperatures & Local Dry Heat Loss*

Although examining thermal windows and regional heterothermy is straightforward with IRT, arriving at a how surface temperatures inform about temperature regulation requires a more theoretical approach.  The standard model for metabolic heat production in endotherms predicts a region of ambient temperatures over which metabolic rate is constant, called the thermoneutral zone (Figure 14).  Below a lower critical temperature (LCT), metabolic rate rises linearly due to increases in heat production required to maintain constant T$_b$.  Above an upper critical temperature (UCT), metabolic rate also may also rises due to metabolism associated with evaporative thermolytic responses.  Within the thermoneutral zone, cardiovascular control over heat distribution to the periphery is responsible for the relatively constant metabolic rates within the thermoneutral zone.  Dry heat loss (*i.e.,* non-evaporative heat transfer) itself is usually analysed using physical models related to convective and conductive heat exchange, whereby a temperature gradient (Δ*T*) determines the rate of heat transfer, with a state or object dependent thermal transfer coefficient (*h*):

$$Q = h(T_1 - T_2)$$

In the case of an endotherm under steady state conditions, the external heat flow ($Q_e$; $W \cdot m^{-2}$) from a particular surface (appendage or otherwise) to the environment and the simultaneous internal heat flow ($Q_i$; $W \cdot m^{-2}$) from the blood to the surface can be estimated as:

$$Q_e = h_e A (T_{surface} - T_{air})$$
$$Q_i = h_i A (T_{blood} - T_{surface})$$

where $h_e$ is influenced by the presence of external insulation, wind speed, and size and shape of the surface. For naked surfaces, $h_e$ is not affected by insulation, and at low wind speeds can be assumed to be influenced primarily by the surface area for heat loss itself. $h_i$ is slightly more complicated, however, since it depends on the amount of blood flowing to the surface, which is under physiological control. Determining the precise values for $Q_e$ and $Q_i$, as well as the heat transfer coefficients may prove challenging, however, these relationships are still informative under steady state conditions, where $Q_e$ should be equal to $Q_i$. In steady state, heat arriving to a surface is the same as heat leaving that surface, which allows for the estimation of relative changes in the internal and external heat transfer coefficients ($h_i$ and $h_e$), as well as overall patterns in $T_{surface}$. The surface temperature can be solved by re-arranging the two equations above (Jessen, 2001), and seen to be a linear function of air and artery temperature, as well as the heat transfer coefficients:

$$T_{surface} = \left( \frac{h_e}{h_e + h_i} \right) T_{air} + \left( \frac{h_i}{h_e + h_i} \right) T_{artery}$$

This relationship allows one to model an endotherm's surface temperature response to changing ambient temperature, as well as examine reasons for regional changes in surface temperature (Figure 15). First, since neither $h_i$ nor $h_e$ can be negative, $T_{surface}$ will never be lower than $T_{air}$ in steady state (ignoring evaporative heat loss). It can also be predicted that if the internal heat flow is high, $h_i \gg h_e$, such that $h_e / (h_e + h_i)$ approaches zero and $T_{surface}$ will primarily be a function of artery temperature, which is nearly constant in an endothermic homeotherm (*i.e.,* slope of $T_{surface}$ vs. $T_{air}$ is close to zero). On the other hand, when external convection predominates and $h_e \gg h_i$, then $h_i / (h_e + h_i)$ approaches zero, and thus $T_{surface}$ will be dependent primarily on $T_{air}$ (*i.e.,* slope of $T_{surface}$

37

vs. $T_{air}$ is closer to one). Re-arranging the $T_{surface}$ equation above to solve for $h_i:h_e$ yields the following:

$$\frac{h_i}{h_e} = \frac{\left(\left[T_a/T_s\right] - 1\right)}{\left(1 - \left[T_{artery}/T_s\right]\right)}$$

where this ratio depicts the relative blood flow to a given body surface. In order to simplify interpretation, one could assume that $T_{artery}$ is constant and equivalent to the average body temperature. Since the temperature values listed above are usually measured in thermoregulatory studies, the $h_i:h_e$ could be calculated relatively easily and used to infer relative changes in blood flow to appendages (Figure 15).

Eyes and the peripalpebral region around the eyes are generally well vascularized, and should tend to have high $h_i:h_e$ at all ambient temperatures. Adjustable thermal windows (such as the bird bill) should show $h_i:h_e$ rising within the thermoneutral zone. Insulating surfaces, on the other hand, should show low $h_i:h_e$ ratios since the potential for regulating blood flow beneath these surfaces is low compared to the potential effects of external factors like air flow and insulation disruption. In previous work, these surface temperatures have generally only been analysed for their correlation to ambient temperature (Klir et al., 1990; Tattersall et al., 2009), although the approach described here could facilitate comparative research. The utility of this approach to evolutionary physiology would be in better understanding Allen's Rule, a phenomenon of endotherm thermal physiology (Allen, 1877; Symonds and Tattersall, 2010). Allen's Rule is the observation that appendages of birds and mammals are relatively smaller in those species living in cold environments, which could result from differential rates of growth (Serrat, 2013) or because of a thermoregulatory adaptation to conserve energy (Tattersall et al., 2012). These questions could be tested using IRT under controlled conditions and comparing species differences in patterns of surface temperatures; $h_e$ is primarily affected by appendage size or shape, while changes in $h_i$ would be indicative of differences in peripheral perfusion. Since surface temperature is readily estimated using modern thermal imaging techniques (Tattersall and Cadena, 2010), by manipulating the air temperature and assuming blood temperature remains constant and close to body

temperature ($\pm 1°C$), the threshold temperature ($T_{thres}$) where $h_i{:}h_e$ begins to rise should correspond to the ambient temperature at which an endotherm begins to recruit vasodilatory mechanisms to their appendages; in other words, the $T_{thres}$ corresponds to the transition temperature above which peripheral blood flow is elevated to the body's thermal windows. In principle, therefore, these three parameters could be assessed using IRT in combination with morphological studies showing appendage size dependency on ambient temperatures. Unfortunately, to the best of my knowledge, no comprehensive study exists that has examined interspecific variation in the above physiological parameters for thermal windows, nor the evolutionary constraints that have influenced these parameters. Limited information exists regarding the actual air temperatures at which thermal windows are recruited, however, one comparative study suggests that smaller mammals (*i.e.,* endotherms) are much more reliant on vasomotor control for the regulation of heat loss, whereas large mammals make use of their large size, and low surface area:volume ratio to minimize overall heat loss (Mortola, 2013; Phillips and Heath, 1995). One would predict from this study that larger birds and mammals would exhibit lower threshold temperatures, and by extension, the reliance a particular species has on utilizing peripheral mechanisms for heat exchange to vary with environmental conditions and evolutionary history.

The approach described here requires an estimate of body temperature and an assumption of constant blood temperature below each surface. Since thermal imaging is often used to substitute for more invasive measures of internal core temperatures, caution is recommended in applying this to situations where $T_b$ is expected to change, since this violates the steady state assumptions of the thermal model. However, $T_b$ values from published work could be used in order to estimate the relative change in these heat transfer coefficients. The estimates will also have greater error at higher ambient temperatures as the denominator approaches zero under these conditions, while the accuracy in $T_b$ estimation remains a constant.

## 5. Conclusions and Perspectives

IRT is a diverse and non-invasive approach to surface temperature assessment in animals and is reasonable simple to use. Most modern imaging devices are as simple as

normal digital cameras in their use yet provide access to direct information about temperature, and in some cases, estimates of relative changes in blood flow. For most applications in physiology the challenges of using IRT accurately are minimal, but generally limited to situations where imaging cameras can be placed in the same environment as the animal to minimise atmospheric attenuation and inherent errors. In combination with existing technologies such as laser Doppler blood flow, computed tomography, or biotelemetry, IRT could further enhance the information gathered by providing dynamic information on surface temperature changes that are due to physiological processes. As a discipline, the field of IRT has traditionally been dominated primarily by applications in physics and engineering, and has only recently been explored mechanistically in the field of physiology. Coupled with computerized imaging analysis and mathematical modeling, IRT could provide new and exciting information on animals engaging in normal behaviours. As more physiologists take their questions to the field and as more ecologists adopt portable technology and modeling in their research, IRT also serves to bring disciplines together and may assist in solving some of the more challenging questions of the future.

## Figure Legends

**Figure 1.** Blackbody spectral radiation according to Stefan-Boltzmann/Planck's law. Spectral Radiance is plotted to the quarter power (on a log-axis) to allow shape comparisons of all the curves. The maximum spectral radiance for each blackbody temperature is shown in the solid black line, according to Wein's law. Visible wavelengths are shown as the rainbow region (390 – 700 nm), Medium Wave Infrared wavelengths (MWIR; 3-5 μm) are shown in dark grey and Long Wave Infrared wavelengths (LWIR; 8-12 μm).

**Figure 2.** Radiation concepts of emissivity, reflectivity, absorptivity and transmissivity. The top panel (A) depicts a simplified model of the fate of incoming radiation (*i*) on a grey body. A portion of incoming radiation can be reflected (*r*), absorbed (*a*), or transmitted (*t*) through a grey body, although *t* is usually negligible, and thus $i = a + r$. According to Kirschoff's radiation law, in thermodynamic equilibrium, the amount of radiation emitted (*e*) must be equivalent to the radiation absorbed, and thus *e* is usually equal to $a = i - r$, meaning that there is generally an inverse relationship between an object's emissivity and reflectivity. The bottom panel (B) illustrates the Stefan-Boltzmann's relationship for a grey body of different emissivities (0.9 and 0.95) compared to a blackbody with emissivity of 1.0.

**Figure 3.** Biological surfaces typically have high emissivities. Wolf fur, a turkey feather, and a Nautilus shell were equilibrated to low (A, ~5°C) and elevated temperatures (B, ~50°C) and then rapidly imaged under a reflected temperature environment of 18°C. Dotted lines indicate the superficial location of a strip of black electrical tape ($\varepsilon$~0.97), which is virtually indistinguishable from the biological materials. Fur and feathers are estimated to have an emissivity of 0.96, and the shell to have an emissivity of 0.96 with this approach.

**Figure 4.** Typical path-flow information and influences on estimates of temperature in infrared thermal imaging. Radiation emanating from an object may include reflected

radiation from the environment, may be attenuated by atmospheric conditions (*e.g.,* humidity) or artificial windows with transmissions <1 before passing through the lens and detected by the sensor. Radiation detected by the sensor is a raw voltage proportional to the radiative flux, and digitized for storage (8 to 16 bits) in a radiometric image file. Usually, camera calibration information is stored with the file, so that the raw radiance signal can be converted offline to an estimated temperature using mathematical algorithms incorporating information from the path-flow analysis. Thermal images stored without radiometric information are typically limited to 8 bits of data calculated under the default conditions of the camera, which may not accurately represent the true scene's information.

**Figure 5.** Error in estimated object temperature based on uncertainty in values used in thermal imaging algorithms. In A, the true object emissivity is 0.95, while the error for two alternative emissivities (1.0 and 0.9) depict how an overestimate and underestimate introduce error in temperature estimation. In B, the reflected temperature (RT) is over and underestimated by 20°C. In C, the relative humidity (RH) is over and under-estimated by 40% for an object at 100 m. In D, the window transmission value ($\tau$) is over and under-estimated by 5%. In all cases, black lines indicate a "true" condition (*i.e.,* zero error), and the red and blue lines represent the effect of an over- and under-estimation of the particular parameter. Unless stated otherwise, actual object temperature is 20°C, distance is 1 m, and surrounding ambient temperature is 20°C.

**Figure 6.** Proper focusing the thermal image ensures accurate temperature estimates. Out of focus images invariably produce an error in estimated object temperature, since when the image is not focused, radiation from the background "bleeds" into the estimated object as would be predicted from simple pixel averaging. In the example shown, the object of interest is always higher than the background temperature. Thermal images of an object situated 1 meter away (D is in focus, E and F are out of focus) were taken in rapid succession at different focus positions (from 0.35 m to ∞ m), and the maximum temperature of the central region estimated. Out of focus images produce an underestimated object temperature, whether the image is under-focused or over-focused,

42

and the larger the object minus background temperature, the larger the error.  In A, the error in estimated temperature of a warm object (44°C) measured at room temperature (23°C) is shown against error in focal distance, whereas B represents the error in estimated temperature of a hot object (90°C) measured at room temperature (23°C).  The worst case underestimation (C) in object temperature is shown to be a monotonic function of the contrast in temperature between object and background ($\Delta$T); larger contrasts lead to a larger error in object temperature.

**Figure 7.** Thermal imager devices and environmental temperatures drift over time.  In the example shown here, the built-in shutter compensation ("self-calibration" option in a FLIR SC 660 was operated as normal (left) and suppressed (right), while recording the temperature inside an insulated box.  The temperature (mean and standard deviation) behind a transparent ($\tau$=0.95) thermal window (internal; expected to be stable) is compared to the temperature outside of the insulated box (external; subject to room temperature drift).  A baseline thermal drift of ~0.099°C is evident over a 30 minute interval inside the insulated box.  The drift in the internal temperature is 2.6 times (0.255°C) greater if the shutter compensation is suppressed; furthermore, the pixel-to-pixel variability also increases without shutter compensation, since each pixel is free to drift randomly (compare sd values).  Circles depict the regions of interest (ROI) of the same number of pixels that were analysed using FLIR ThermaCAM Researcher Pro. Top thermal images represent image subtraction thermograms (final frame − first frame), which if drift were absent would be completely black (0°C for every pixel).  Bottom histograms represent values from the ROIs of the final frame after 1200 s.

**Figure 8.**  Temperature gradient device for assessing thermal preference in lizards. Using a thin copper plate that is heated at one end and cooled at the other end, a linear gradient for floor temperature results allowing small ectotherms, like young lizards to select different ambient temperatures over time.  Thermal image is derived from data published in Khan et al. (2010).

**Figure 9.** Respiratory and rostral cooling accompanies breathing in various reptiles. In A, a basking Argentine black and white tegu lizard (*Salvatore merianae*), in B, a South American tortoise (*Geochelone carbonaria*), in C, a South American rattlesnake (*Crotalus durissus*), and in D, a broad-nosed caiman (*Caiman latirostris*) are shown. Thermal gradients have been removed for simplicity. Thermal images are derived from various sources (Cadena et al., 2013; Tattersall et al., 2006a).

**Figure 10.** Evaporation from the skin leads to cooler surface temperatures in amphibians. In the left panel (A), a small frog (*Bokermannohyla alvarengai*) has been exposed to a brief gust of air, and shows significant cooling below the air temperature. In the right panel (B), the same frog minutes later returning to normal temperatures after evaporative cooling has ceased. Ectotherms like amphibians with moist skin can therefore be readily imaged with thermal imaging as their body temperatures are typically going to be cooler than the prevailing air temperatures. Both panels also demonstrate the influence of emissivity on temperature errors. The floor the frog is resting on is made of aluminum foil, which has a very low emissivity; the reflected temperature on the floor is therefore influenced by overhead lights as well as the thermal camera itself. Thermal image data are unpublished images originating from Tattersall et al. (Tattersall, 2016; Tattersall et al., 2006a; Tattersall et al., 2004).

**Figure 11.** Exotherms arising from the latent heat of fusion of tissue water freezing in supercooled insects can be assessed using thermal imaging. In A, a thermal image is shown depicting a top down view of 8 carpenter bees (*Xylocopa virginica*) being slowly cooled to -25°C within a plastic cylinder. Three bees can be seen (the remaining 5 are invisible due to being equal to the ambient temperature) in the middle of the process of whole body freezing, which takes nearly 20 minutes. In the centre, a piece of high emissivity foil can be seen reflecting camera temperature which is much higher than floor temperature. In B, a sample trace of the average bee surface temperature and ambient temperature is shown during a spontaneous freezing event. Thermal images and data derived from Skandalis et al. (2006b).

**Figure 12.** Brown adipose tissue (BAT) activity can be imaged in the interscapular region of small rodents. In the top panel (A), a depilated mouse has been injected systemically with nor-epinephrine to simulate sympathetic activation of BAT uncoupling. BAT temperature rises by 1 to 2°C above $T_b$ within 30 minutes following injection. In the bottom panel (B), 9 two-day old neonatal mice (naturally nude) demonstrate evidence of warm BAT temperatures with simply exposure to an air temperature of 28°C. Genetic models (label *ko*) deficient in the capacity to activate BAT show little to no evidence of interscapular heating. Thermal image data are unpublished images originating from Hodges et al (2011).

**Figure 13.** Surface temperature of the pelage of endotherms reveals differences in insulation capacity. In panel A is shown a thermal image of two dogs (Australian Shephard) outside at 0°C, the one on the left has a congenital lack of undercoat fur and has surface temperatures ~4°C warmer than the one on the right with a thick insulating coat. In B is shown a horse that has had fur clipped in places, revealing surface temperatures that are higher and approaching body temperature.

**Figure 14.** Thermoregulatory control in endotherms involves control over heat production (A) and heat loss (B). Thermogenic heat production is activated below the lower critical temperature (LCT) in a linear fashion. Above the LCT, endotherms maintain constant metabolic heat production within the thermoneutral zone (TNZ), making use of metabolically neutral processes (primarily peripheral vasomotor changes) to regulate body temperature ($T_b$). The threshold temperature for the activation of vasoactive control on peripheral temperature is expected to occur at the LCT or within the TNZ. Above $T_{thres}$, surface temperatures of the body depend on a combination of blood flow and the property of the surface itself. For body surfaces with high rates of blood flow, $h_i \gg h_e$. Below $T_{thres}$, $h_i$ is negligible and surface temperatures are primarily a function of air temperature, and thus heat loss is severely curtailed.

**Figure 15.** Regional variation in surface temperatures of an endotherm follows on from changes in the ratio of internal to external heat flow with changes in ambient temperature.

The left panels show actual $h_i$:$h_e$ ratios (grey area shows minimum and maximum values) for different regions of the body surface (A, eye; B, proximal bill; C, distal bill; D, feather temperatures). Sample thermal images of a toco toucan (*Ramphastos toco*) are shown at different ambient temperatures (E, 15°C; F, 25°C; and G, 35°C). With increasing ambient temperature, as the gradient between $T_{surface}$ and $T_a$ decreases, the $h_i$:$h_e$ generally increases, especially within the thermoneutral zone. Regions with higher blood flow rates are predicted to have large $h_i$:$h_e$ as well as large changes in $h_i$:$h_e$. Since $T_{surface}$ must be equal to or greater than $T_a$, a slope of the $T_{surface}$ *vs.* $T_a$, as performed in earlier studies (2008) shows its inverse relationship to the $h_i$:$h_e$ (panel H). For reference, dotted lines depict where the $h_i$:$h_e$ is equal to 1. Thermal image data are re-analysed data derived from Tattersall et al. (Tattersall et al., 2004).

47

## Acknowledgements

## References

Abramoff, M.D., Magalhaes, P.J., Ram, S.J., 2004. Image processing with ImageJ. Biophotonics International 11, 36-42.

Al-Nakhli, H.H., Petrofsky, J.S., Laymon, M.S., Berk, L.S., 2012. The use of thermal infra-red imaging to detect delayed onset muscle soreness. Jove-Journal of Visualized Experiments.

Allen, J.A., 1877. The influence of physical conditions in the genesis of species. Radical Review 1, 108-140.

Almeida, M.C., Steiner, A.A., Branco, L.G.S., Romanovsky, A.A., 2006. Cold-seeking behavior as a thermoregulatory strategy in systemic inflammation. European Journal of Neuroscience 23, 3359-3367.

Berz, R., Sauer, H., 2007. The medical use of infrared-thermography history and recent applications. Thermografie-Kolloquium 4, 1-12.

Best, R.G., Fowler, R., 1981. Infrared emissivity and radiant surface temperatures of Canada and snow geese. Journal of Wildlife Management 45, 1026-1029.

Betke, M., Hirsh, D.E., Makris, N.C., Mccracken, G.F., Procopio, M., Hristov, N.I., Tang, S., Bagchi, A., Reichard, J.D., Horn, J.W., Crampton, S., Cleveland, C.J., Kunz, T.H., 2008. Thermal imaging reveals significantly smaller Brazilian free-tailed bat colonies than previously estimated. Journal of Mammalogy 89, 18-24.

Blaxter, K., 1989. Energy metabolism in animals and man. Cambridge University Press, Cambridge.

Blumberg, M.S., Deaver, K., Kirby, R.F., 1999. Leptin disinhibits nonshivering thermogenesis in infants after maternal separation. American Journal of Physiology-Regulatory Integrative and Comparative Physiology 276, R606-R610.

Blumberg, M.S., Efimova, I.V., Alberts, J.R., 1992. Thermogenesis during ultrasonic vocalization by rat pups isolated in a warm environment - a thermographic analysis. Developmental Psychobiology 25, 497-510.

Blumberg, M.S., Lewis, S.J., Sokoloff, G., 2002. Incubation temperature modulates post-hatching thermoregulatory behavior in the Madagascar ground gecko, *Paroedura pictus*. Journal of Experimental Biology 205, 2777-2784.

Boonstra, R., Eadie, J.M., Krebs, C.J., Boutin, S., 1995. Limitations of far-infrared thermal imaging in locating birds. Journal of Field Ornithology 66, 192-198.

Boonstra, R., Krebs, C.J., Boutin, S., Eadie, J.M., 1994. Finding mammals using far-infrared thermal imaging. Journal of Mammalogy 75, 1063-1068.

Borrell, B.J., LaDuc, T.J., Dudley, R., 2005. Respiratory cooling in rattlesnakes. Comparative Biochemistry and Physiology A 140, 471-476.

Bouma, H.R., Verhaag, E.M., Otis, J.P., Heldmaier, G., Swoap, S.J., Strijkstra, A.M., Henning, R.H., Carey, H.V., 2012. Induction of torpor: Mimicking natural metabolic suppression for biomedical applications. Journal of Cellular Physiology 227, 1285-1290.

Buchholz, R., 1996. Thermoregulatory role of the unfeathered head and neck in male wild turkeys. Auk 113, 310-318.

Cabanac, M., Gosselin, F., 1993. Emotional fever in the lizard *Callopistes maculatus* (Teiidae). Animal Behaviour 46, 200-202.

Cadena, V., Tattersall, G.J., Bovo, R., Andrade, D.V., 2013. Evaporative respiratory cooling augments pit organ thermal detection in rattlesnakes. Journal of Comparative Physiology A 199, 1093-1104.

Dawson, C., Vincent, J.F.V., Jeronimidis, G., Rice, G., Forshaw, P., 1999. Heat transfer through penguin feathers. Journal of Theoretical Biology 199, 291-295.

Dunkin, R.C., McLellan, W.A., Blum, J.E., Pabst, D.A., 2005. The ontogenetic changes in the thermal properties of blubber from Atlantic bottlenose dolphin *Tursiops truncatus*. Journal of Experimental Biology 208, 1469-1480.

Dzialowski, E.M., Tattersall, G.J., Nicol, S.C., Frappell, P.B., 2014. Fluctuations in oxygen influence facultative endothermy in bumblebees. Journal of Experimental Biology 217, 3834-3842.

Faye, E., Dangles, O., Pincebourde, S., 2016. Distance makes the difference in thermography for ecological studies. Journal of Thermal Biology 56, 1-9.

Faye, E., Rebaudo, F., Yánez-Cajo, D., Cauvy-Fraunié, S., Dangles, O., 2015. A toolbox for studying thermal heterogeneity across spatial scales: from unmanned aerial vehicle imagery to landscape metrics. Methods in Ecology and Evolution In Press.

FLIR, 2007. The ultimate infrared handbook for R&D professionals, 160.

Florant, G.L., Heller, H.C., 1977. CNS regulation of body temperature in euthermic and hibernating marmots (*Marmota flaviventris*). American Journal of Physiology 232, R203-R208.

Gallegoa, B., Verdúa, J.R., Carrascalb, L.M., Lobob, J.M., 2016. A protocol for analysing thermal stress in insects using infrared thermography. Journal of Thermal Biology 56, 113-121.

Garrick, D., 2008. Body surface temperature and length in relation to the thermal biology of lizards. Bioscience Horizons 1, 136-142.

Gates, D.M., 2003. Biophysical Ecology, Dover Books on Biology Ser. Dover Publications, Incorporated, Mineola, 656.

Gerken, M., 1997. Application of infra-red thermography to evaluate the influence of the fibre on body surface temperature in llamas. European Fine Fibre Network 6, 65-71.

Greenberg, R., Cadena, V., Danner, R.M., Tattersall, G.J., 2012. Heat loss may explain bill size differences between birds occupying different habitats. Plos One 7, e40933.

Hagan, A.A., Heath, J.E., 1980. Regulation of heat loss in the duck by vasomotion in the bill. Journal of Thermal Biology 5, 95-101.

Hammel, H.T., 1956. Infrared emissivities of some arctic fauna. Journal of Mammalogy 37, 375-378.

Heller, H.C., Hammel, H.T., 1971. CNS regulation of body temperature in the hibernator *Citellus lateralis*. International Journal of Biometeorology 15, 231-235.

Heller, H.C., Hammel, H.T., 1972. CNS control of body temperature during hibernation. Comparative Biochemistry and Physiology A 41, 349-359.

Hildebrandt, C., Raschner, C., Ammer, K., 2010. An overview of recent application of medical infrared thermography in sports medicine in Austria. Sensors 10, 4700-4715.

Hill, R.W., Christian, D.P., Veghte, J.H., 1980. Pinna temperature in exercising jackrabbits, *Lepus californicus*. Journal of Mammalogy 61, 30-38.

Hill, R.W., Veghte, J.H., 1976. Jackrabbit ears - surface temperatures and vascular responses. Science 194, 436-438.

Hillman, S.S., Hedrick, M.S., 2015. A meta-analysis of in vivo vertebrate cardiac performance: implications for cardiovascular support in the evolution of endothermy. Journal of Experimental Biology 218, 1143-1150.

Hodges, M.R., Tattersall, G.J., Harris, M.B., McEvoy, S.D., Richerson, D.N., Deneris, E.S., Johnson, R.L., Chen, Z.F., Richerson, G.B., 2008. Defects in breathing and thermoregulation in mice with near-complete absence of central serotonin neurons. Journal of Neuroscience 28, 2495-2505.

Holst, G.C., 2000. Common sense approach to thermal imaging. SPIE Optical Engineering Press; JCD Publishing, Bellingham, Wash & Winter Park, Fla.

Jackson, D.M., Hambly, C., Trayhurn, P., Speakman, J.R., 2001. Can non-shivering thermogenesis in brown adipose tissue following NA injection be quantified by changes in overlying surface temperatures using infrared thermography? Journal of Thermal Biology 26, 85-93.

Jessen, C., 2001. Temperature Regulation in Humans and Other Animals. Springer-Verlag, Berlin, Germany.

Jones, B.F., 1998. A reappraisal of the use of infrared thermal image analysis in medicine. IEEE Trans Med Imaging 17, 1019-1027.

Kerr, 2004. Review of the effectiveness of infrared thermal imaging (thermography) for population screening and diagnostic testing of breast cancer. NZHTA Tech Brief Series 3, 3.

Khan, J.J., Richardson, J.M.L., Tattersall, G.J., 2010. Thermoregulation and aggregation in neonatal bearded dragons (*Pogona vitticeps*). Physiology & Behavior 100, 180-186.

Klir, J.J., Heath, J.E., 1994. Thermoregulatory responses to thermal stimulation of the preoptic anterior hypothalamus in the red fox (*Vulpes vulpes*). Comparative Biochemistry and Physiology A 109, 557-566.

Klir, J.J., Heath, J.E., Bennani, N., 1990. An infrared thermographic study of surface temperature in relation to external thermal stress in the Mongolian gerbil, *Meriones unguiculatus*. Comparative Biochemistry and Physiology A 96, 141-146.

Kouba, A., 2005. What's new and hot in zoo technology: Thermography.

Kovac, H., Stabentheiner, A., Hetz, S.K., Petz, M., Crailsheim, K., 2007. Respiration of resting honeybees. Journal of Insect Physiology 53, 1250-1261.

Kvadsheim, P.H., Folkow, L.P., Blix, A.S., 1994. A new device for measurement of the thermal conductivity of fur and blubber. Journal of Thermal Biology 19, 431-435.

Lancaster, W.C., Thomson, S.C., Speakman, J.R., 1997. Wing temperature in flying bats measured by infrared thermography. Journal of Thermal Biology 22, 109-116.

Lane, B., Whitenton, E., Madhavan, V., Donmez, A., 2013. Uncertainty of temperature measurements by infrared thermography for metal cutting applications. Metrologia 50, 637-653.

Lathlean, J., Seuront, L., 2014. Infrared thermography in marine ecology: methods, previous applications and future challenges. Marine Ecology Progress Series 514, 263-277.

Maloney, S.K., Dawson, T.J., 1994. Thermoregulation in a large bird, the Emu (*Dromaius novaehollandiae*). Journal of Comparative Physiology B-Biochemical Systemic and Environmental Physiology 164, 464-472.

Mapalad, K.S., Leu, D., Nieh, J.C., 2008. Bumble bees heat up for high quality pollen. Journal of Experimental Biology 211, 2239-2242.

Matis, G., Grigor, J., James, J., McHugh, S., Bryane, P., 2006. Radiance calibration of target projectors for infrared testing. Infrared Imaging Systems: Design, Analysis, Modeling, and Testing XVII 6207, N2070-N2070.

MATLAB, 2015. MATLAB and Image Processing Toolbox. The MathWorks, Inc., Natick, Massachusetts, United States.

Mauck, B., Bilgmann, K., Jones, D.D., Eysel, U., Dehnhardt, G., 2003. Thermal windows on the trunk of hauled-out seals: hot spots for thermoregulatory evaporation? Journal of Experimental Biology 206, 1727-1738.

McCafferty, D.J., 2007. The value of infrared thermography for research on mammals: previous applications and future directions. Mammal Review 37, 207-223.

McCafferty, D.J., Gilbert, C., Thierry, A.M., Currie, J., Le Maho, Y., Ancel, A., 2013. Emperor penguin body surfaces cool below air temperature. Biology Letters 9.

McNab, B.K., 2001. Energetics of toucans, a barbet, and a hornbill: Implications for avian frugivory. Auk 118, 916-933.

Michel, C., Frankham, P., Cabanac, M., 2003. Salicylate as a partial inhibitor of emotional fever and body weight set-point in rats: behavioral and neuroendocrine study. Physiology & Behavior 78, 357-363.

Midtgard, U., 1980. Arteriovenous anastomoses and vascularity in the feet of eiders and gulls (Aves). Zoomorphology 96, 263-270.

Midtgard, U., 1984. Blood vessels and the occurrence of arteriovenous anastomoses in cephalic heat loss areas of mallards, *Anas platyrhynchos* (Aves). Zoomorphology 104, 323-335.

Minkina, W., Dudzik, S., 2009. Infrared thermography errors and uncertainties. J. Wiley, Chichester, West Sussex, U.K. ; Hoboken, NJ, xix, 192 p.

Mohler, F.S., Heath, J.E., 1988. Comparison of IR thermography and thermocouple measurement of heat loss from rabbit pinna. American Journal of Physiology-Regulatory Integrative and Comparative Physiology 254, R389-395.

Monteith, J.L., Mount, L.E., 1974. Heat loss from animals and man : assessment and control ; proceedings of the twentieth Easter School in Agricultural Science, University of Nottingham, 1973. Butterworths, London.

Moritz, G.L., Dominy, N.J., 2012. Thermal imaging of aye-ayes (*Daubentonia madagascariensis*) reveals a dynamic vascular supply during haptic sensation. International Journal of Primatology 33, 588-597.

Morrison, P., 1966. Insulative flexibility in the Guanaco. Journal of Mammalogy 47, 18-23.

Mortola, J.P., 2013. Thermographic analysis of body surface temperature of mammals. Zoological Science 30, 118-124.

Munn, A.J., Barboza, P.S., Dehn, J., 2009. Sensible heat loss from Muskoxen (*Ovibos moschatus*) feeding in winter: Small calves are not at a thermal disadvantage compared with adult cows. Physiological and Biochemical Zoology 82, 455-467.

Norris, A.L., Houser, D.S., Crocker, D.E., 2010. Environment and activity affect skin temperature in breeding adult male elephant seals (*Mirounga angustirostris*). Journal of Experimental Biology 213, 4205-4212.

Osborne, P.G., Sato, J., Shuke, N., Hashimoto, M., 2005. Sympathetic alpha-adrenergic regulation of blood flow and volume in hamsters arousing from hibernation. American Journal of Physiology-Regulatory Integrative and Comparative Physiology 289, R554-R562.

Otsuka, K., Togawa, T., 1997. Hippocratic thermography. Physiol Meas 18, 227-232.

Palmer, C.M., Siebke, K., Yeates, D.K., 2004. Infrared video thermography: a technique for assessing cold adaptation in insects. Biotechniques 37, 212-217.

Phillips, P.K., Heath, J.E., 1992. Heat exchange by the pinna of the african elephant (*Loxodonta africana*). Comparative Biochemistry and Physiology, Part A: Molecular & Integrative Physiology 101, 693-699.

Phillips, P.K., Heath, J.E., 1995. Dependency of surface temperature regulation on body size in terrestrial mammals. Journal of Thermal Biology 20, 281-289.

Phillips, P.K., Heath, J.E., 2004. Comparison of surface temperature in 13-lined ground squirrel (*Spermophilus tridecimlineatus*) and yellow-bellied marmot (*Marmota flaviventris*) during arousal from hibernation. Comparative Biochemistry and Physiology a-Molecular & Integrative Physiology 138, 451-457.

Phillips, P.K., Sanborn, A.F., 1994. An infrared, thermographic study of surface-temperature in 3 ratites - ostrich, emu and double wattled cassowary. Journal of Thermal Biology 19, 423-430.

Picard, K., Thomas, D.W., Festa-Bianchet, M., Lanthier, C., 1994. Bovid horns: an important site for heat loss during winter? Journal of Mammalogy 75, 710-713.

Pincebourde, S., Sanford, E., Helmuth, B., 2009. An intertidal sea star adjusts thermal inertia to avoid extreme body temperatures. American Naturalist 174, 890-897.

Powers, D.R., Tobalske, B.W., Langland, K.M., Wethington, S.M., Wilson, J.K., Woods, H.A., 2015. Heat dissipation during hovering and forward flight in hummingbirds and the potential impact of climate change. Integrative and Comparative Biology 55, E145-E145.

Proulx, T.A., 2011. Thermomechanics and infra-red imaging. Volume 7 proceedings of the 2011 Annual Conference on Experimental and Applied Mechanics, Conference Proceedings of the Society for Experimental Mechanics. Springer, New York, viii, 129 pages.

Rodriguez, J.M., Ustin, S.L., Riano, D., 2011. Contributions of imaging spectroscopy to improve estimates of evapotranspiration. Hydrological Processes 25, 4069-4081.

Rogalski, A., 2012. History of infrared detectors. Opto-Electronics Review 20, 279-308.

Romanovsky, A.A., Ivanov, A.I., Shimansky, Y.P., 2002. Molecular biology of thermoregulation - Selected contribution: Ambient temperature for experiments in rats: a new method for determining the zone of thermal neutrality. Journal of Applied Physiology 92, 2667-2679.

Rudaya, A.Y., Steiner, A.A., Robbins, J.R., Dragic, A.S., Romanovsky, A.A., 2005. Thermoregulatory responses to lipopolysaccharide in the mouse: dependence on

the dose and ambient temperature. American Journal of Physiology-Regulatory Integrative and Comparative Physiology 289, R1244-R1252.

Serrat, M.A., 2013. Environmental temperature impact on bone and cartilage growth. Comprehensive Physiology 4, 621-655.

Sheahen, T.P., 1983. Effect of atmospheric attenuation on temperature-measurements made using IR scanning systems. Applied Optics 22, 1070-1077.

Skandalis, D., Richards, M., Sformo, T., Tattersall, G., 2011. Climate limitations on the distribution and phenology of a large carpenter bee, *Xylocopa virginica* (Hymenoptera: Apidae). Canadian Journal of Zoology 89, 785-795.

Speakman, J.R., Ward, S., 1998. Infrared thermography: principles and applications. Zoology 101, 224-232.

Stabentheiner, A., Kovac, H., Hetz, S.K., Kafer, H., Stabentheiner, G., 2012. Assessing honeybee and wasp thermoregulation and energetics-New insights by combination of flow-through respirometry with infrared thermography. Thermochimica Acta 534, 77-86.

Stabentheiner, A., Schmaranzer, S., 1987. Thermographic determination of body temperatures in honey bees and hornets: calibration and applications. Thermology 2, 563-572.

Stuginski, D.R., Fernandes, W., Tattersall, G.J., Abe, A.S., 2011. Postprandial thermogenesis in *Bothrops moojeni* (Serpentes: Viperidae). Journal of Venomous Animals and Toxins including Tropical Diseases 89, 287-292.

Sumbera, R., Zelova, J., Kunc, P., Knizkova, I., Burda, H., 2007. Patterns of surface temperatures in two mole-rats (Bathyergidae) with different social systems as revealed by IR-thermography. Physiology & Behavior 92, 526-532.

Symonds, M.R.E., Tattersall, G.J., 2010. Geographical variation in bill size across bird species provides evidence for Allen's rule. American Naturalist 176, 188-197.

Tattersall, G., Sinclair, B., Withers, P., Fields, P., Seebacher, F., Cooper, C., Maloney, S., 2012. Coping with thermal challenges: Physiological adaptations to environmental temperatures. Comprehensive Physiology 2, 2151-2202.

Tattersall, G.J., 2015. Thermimage: Functions for Handling Thermal Images. R package version 1.0.1., http://CRAN.R-project.org/package=Thermimage.

Tattersall, G.J., 2016. Seasonal reproductive endothermy in the tegu lizard. Science Advances In Press.

Tattersall, G.J., Andrade, D.V., Abe, A.S., 2009. Heat exchange from the toucan bill reveals a controllable vascular thermal radiator. Science 325, 468-470.

Tattersall, G.J., Cadena, V., 2010. Insights into animal temperature adaptations revealed through thermal imaging. Imaging Science Journal 58, 261-268.

Tattersall, G.J., Cadena, V., Skinner, M.C., 2006a. Respiratory cooling and thermoregulatory coupling in reptiles. Respiration Physiology and Neurobiology 154, 302-318.

Tattersall, G.J., Eterovick, P.C., de Andrade, D.V., 2006b. Tribute to R.G. Boutilier: Skin colour and body temperature changes in basking *Bokermannohyla alvarengai* (Bokermann 1956). Journal of Experimental Biology 209, 1185-1196.

Tattersall, G.J., Milsom, W.K., 2003. Transient peripheral warming accompanies the hypoxic metabolic response in the golden-mantled ground squirrel. Journal of Experimental Biology 206, 33-42.

Tattersall, G.J., Milsom, W.K., Abe, A.S., Brito, S.P., Andrade, D.V., 2004. The thermogenesis of digestion in rattlesnakes. Journal of Experimental Biology 207, 579-585.

Taylor, C.R., 1966. The vascularity and possible thermoregulatory function of the horns in goats. Physiological Zoology 38, 127-139.

Thompson, C.I., Brannon, A.J., Heck, A.L., 2003. Emotional fever after habituation to the temperature-recording procedure. Physiology & Behavior 80, 103-108.

Tosini, G., Avery, R., 1993. Intraspecific variation in lizard thermoregulatory set points - a thermographic study in *Podarcis muralis*. Journal of Thermal Biology 18, 19-23.

Tosini, G., Avery, R.A., 1994. Occlusion of the parietal eye induces a transient wavelength-dependent shift in lizard thermoregulatory set points. Journal of Experimental Zoology 269, 84-87.

Tosini, G., Jones, S., Avery, R., 1995. Infrared irradiance and set-point temperatures in behaviorally thermoregulating lacertid lizards. Journal of Thermal Biology 20, 497-503.

Turner, T.A., 2001. Diagnostic thermography. Veterinary Clinics of North America: Equine Practice 17, 95-113.

Usamentiaga, R., Venegas, P., Guerediaga, J., Vega, L., Molleda, J., Bulnes, F.G., 2014. Infrared thermography for temperature measurement and non-destructive testing. Sensors 14, 12305-12348.

VanNerum, K., Buelens, H., 1997. Hypoxia-controlled winter metabolism in honeybees (*Apis mellifera*). Comparative Biochemistry and Physiology a-Physiology 117, 445-455.

Verdu, J.R., Alba-Tercedor, J., Jimenez-Manrique, M., 2012. Evidence of different thermoregulatory mechanisms between two sympatric *Scarabaeus* species using infrared thermography and micro-computer tomography. Plos One 7.

Villarreal, J.A., Schlegel, W.M., Prange, H.D., 2007. Thermal environment affects morphological and behavioral development of *Rattus norvegicus*. Physiology & Behavior 91, 26-35.

Wallin, B., 1994. Temperature measurement on and inside lamps. Proceedings of the SPIE 2245, 241-251.

Ward, S., Rayner, J.M., Moller, U., Jackson, D.M., Nachtigall, W., Speakman, J.R., 1999. Heat transfer from starlings *Sturnus vulgaris* during flight. Journal of Experimental Biology 202, 1589-1602.

Wilson, R.P., Adelung, D., Latorre, L., 1998. Radiative heat loss in gentoo penguin (*Pygoscelis papua*) adults and chicks and the importance of warm feet. Physiological Zoology 71, 524-533.

Wisniewski, M., Lindow, S.E., Ashworth, E.N., 1997. Observations of ice nucleation and propagation in plants using infrared video thermography. Plant Physiology 113, 327-334.
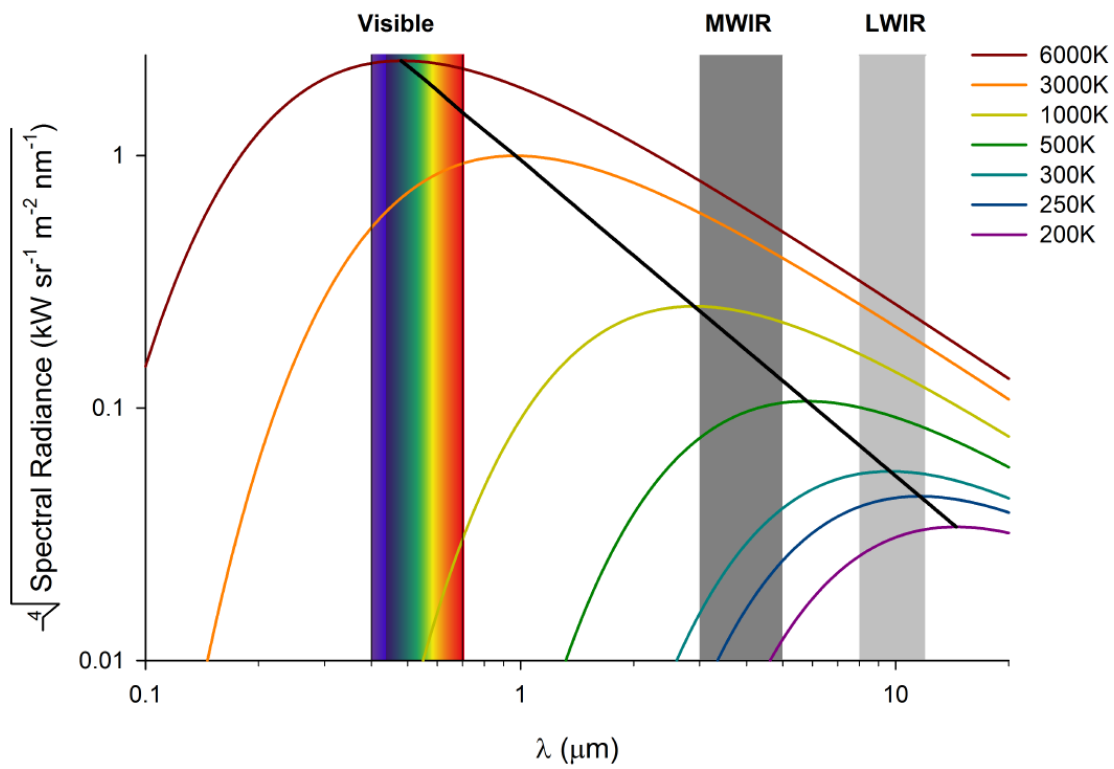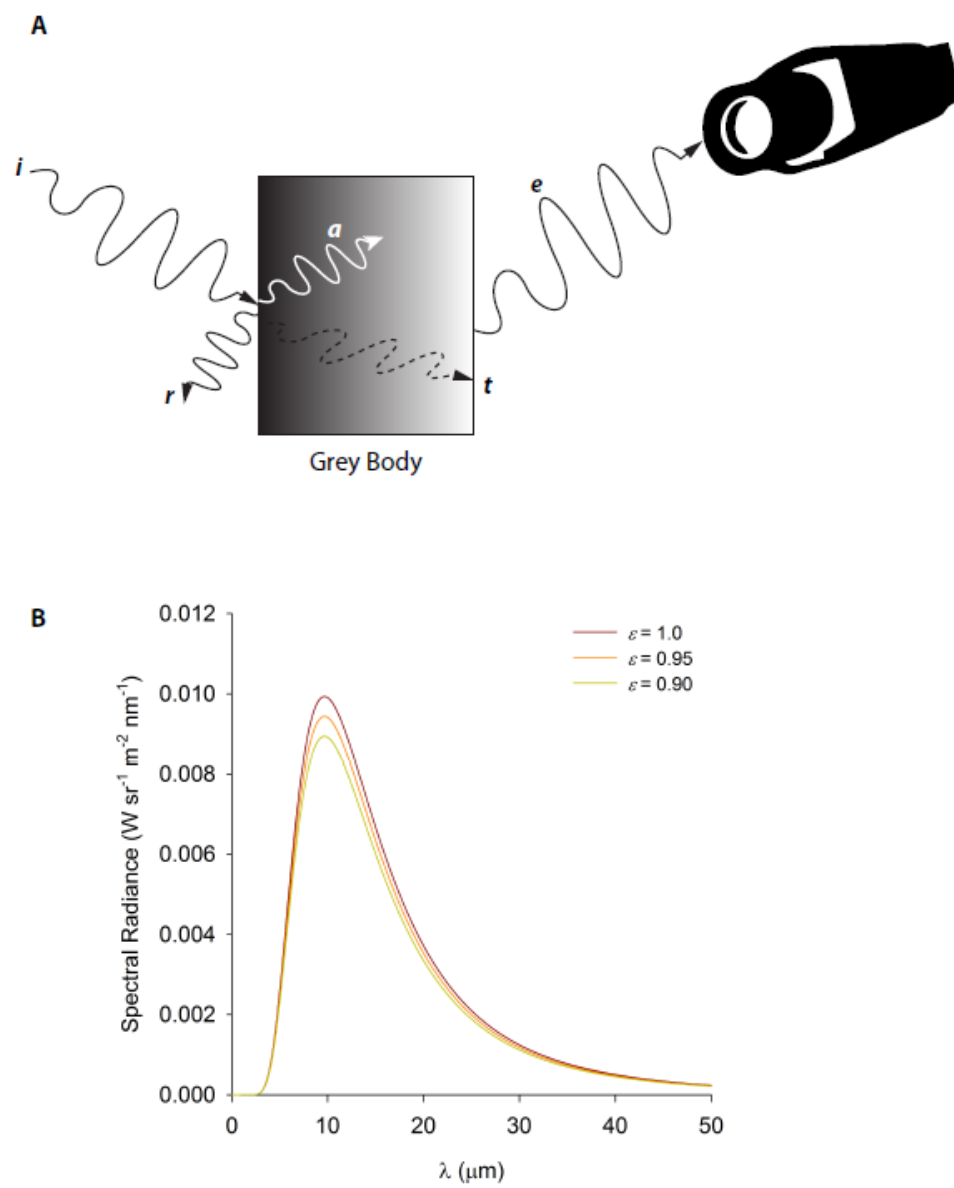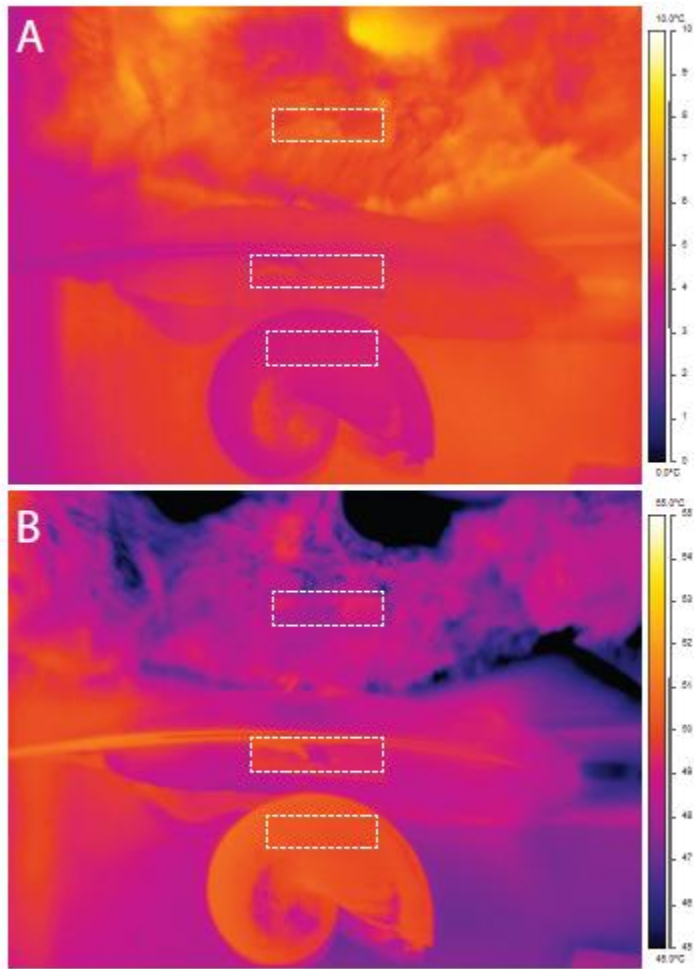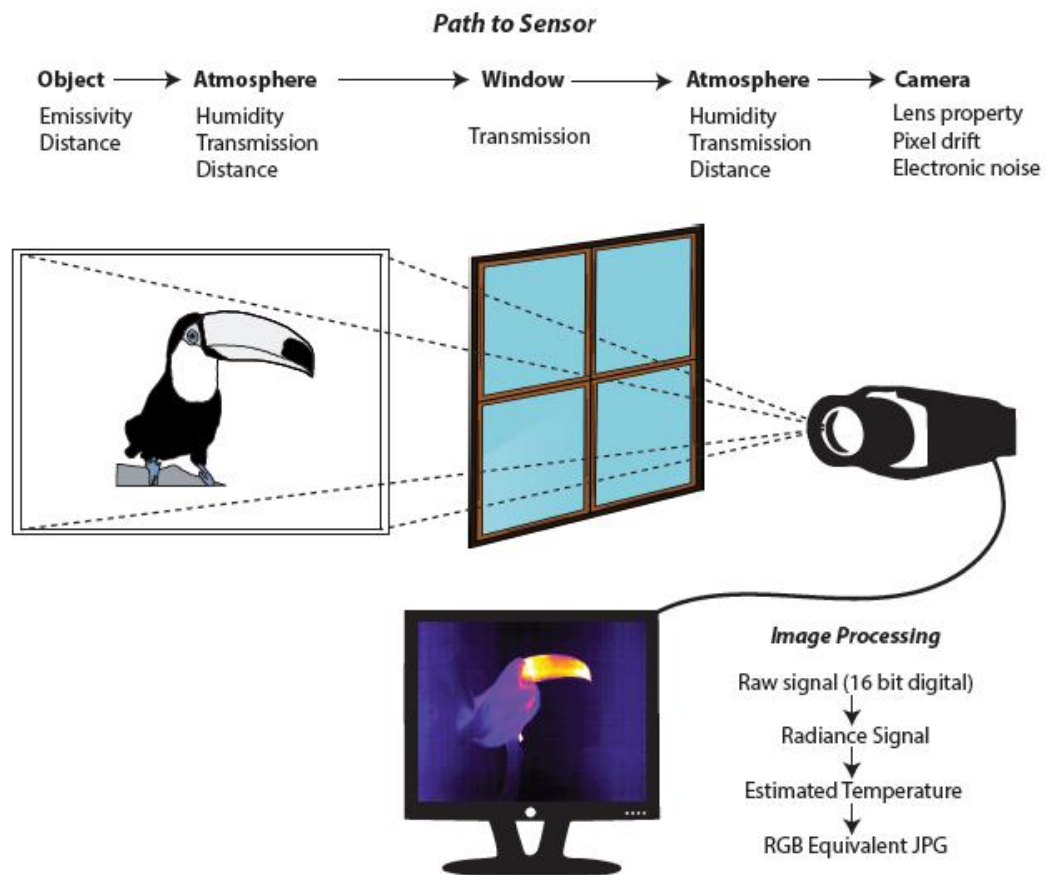
Fig. 1

Fig. 2

Fig. 3

Fig. 4
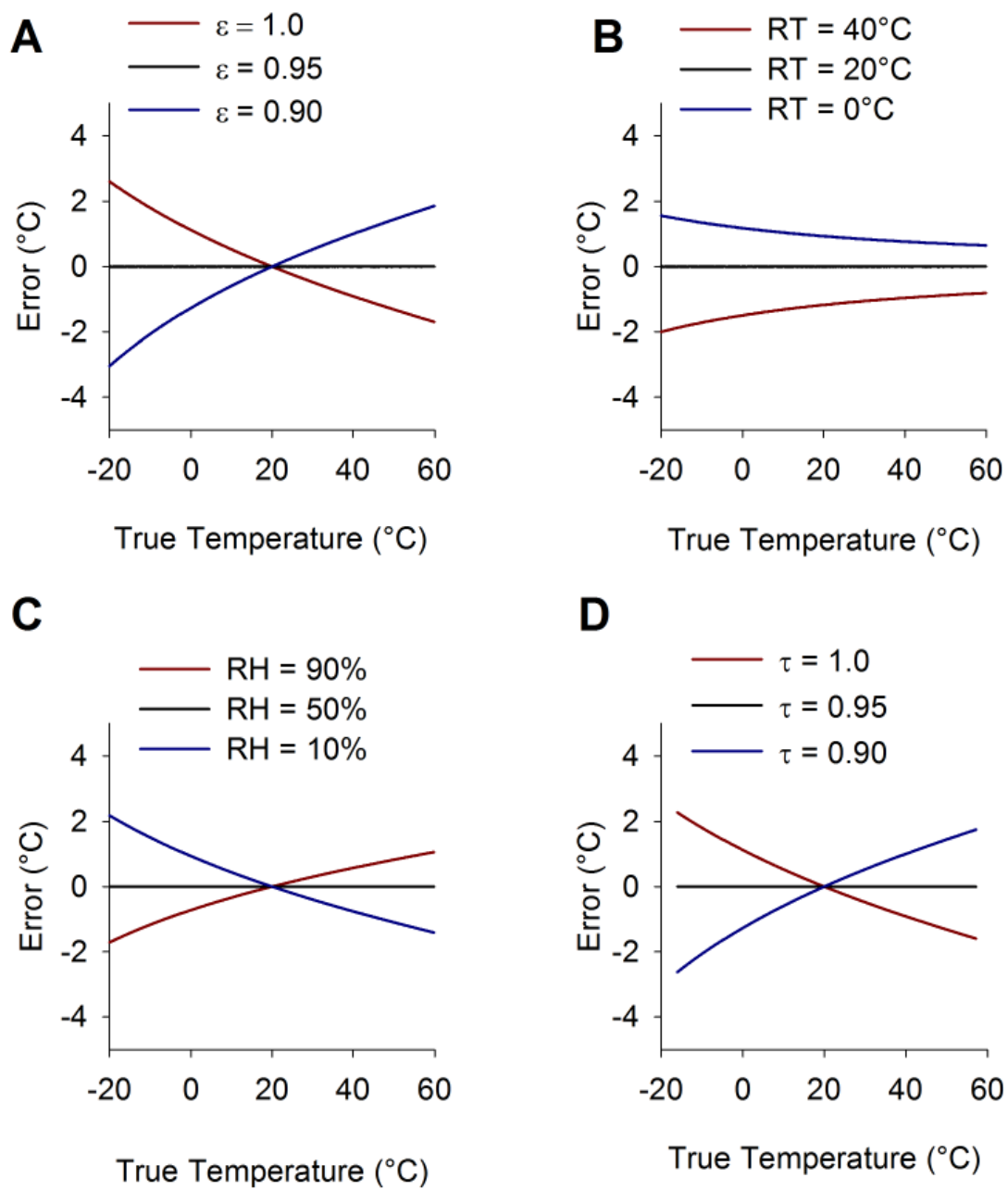
Fig. 5

Fig. 6

Fig. 7

Fig. 8

Fig. 9

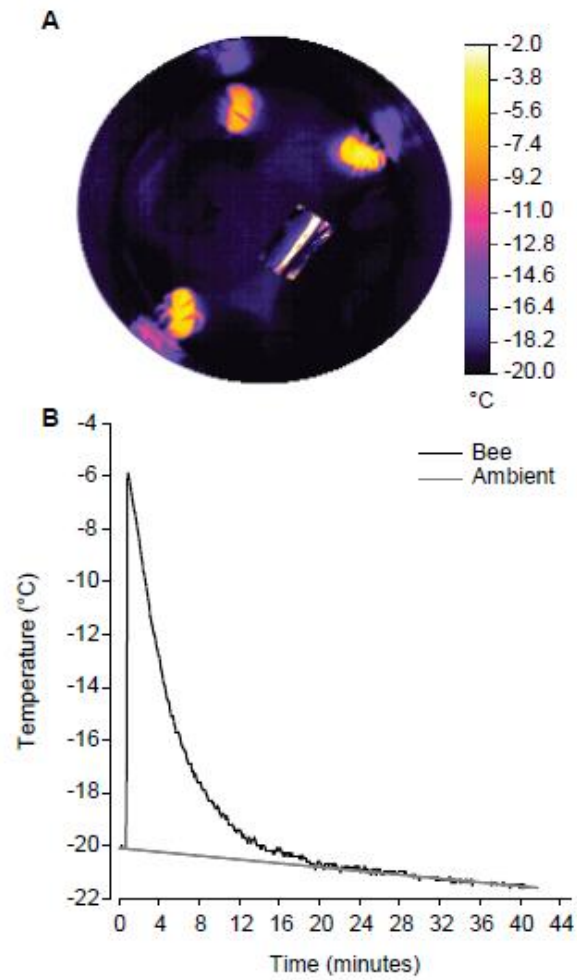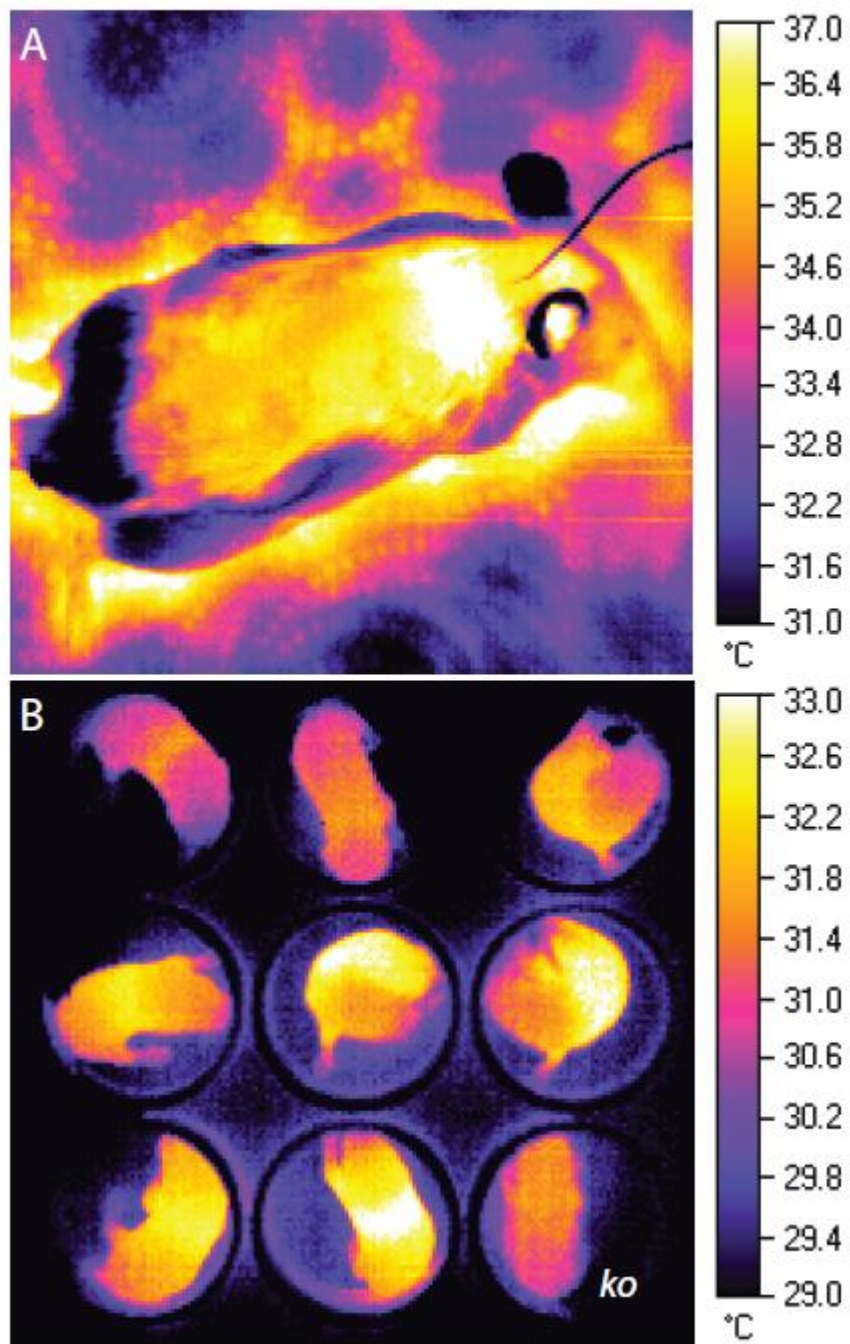64
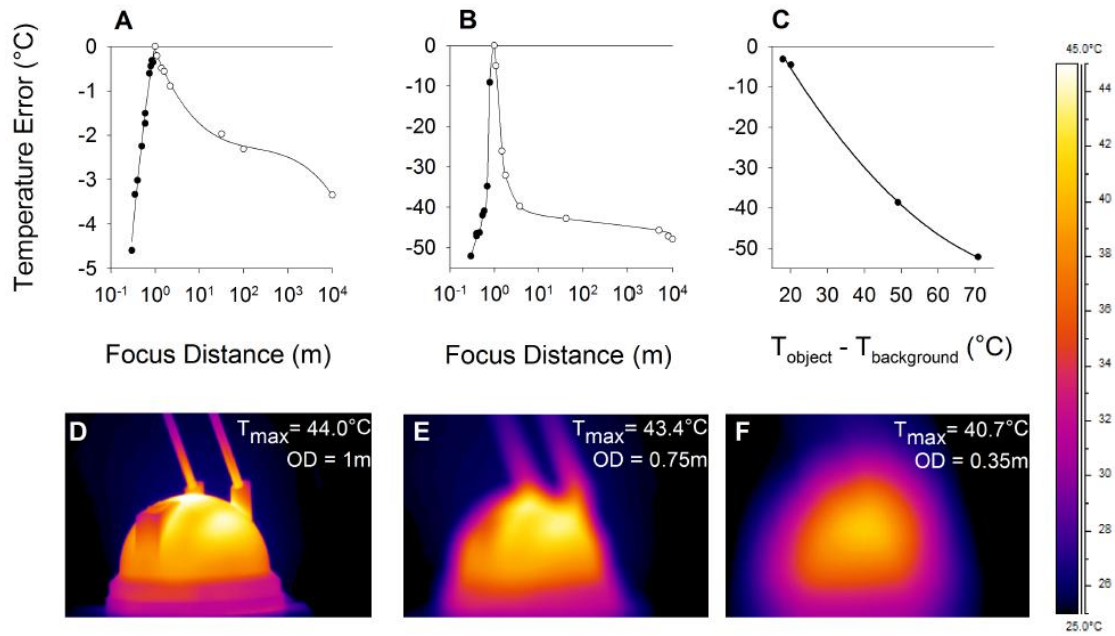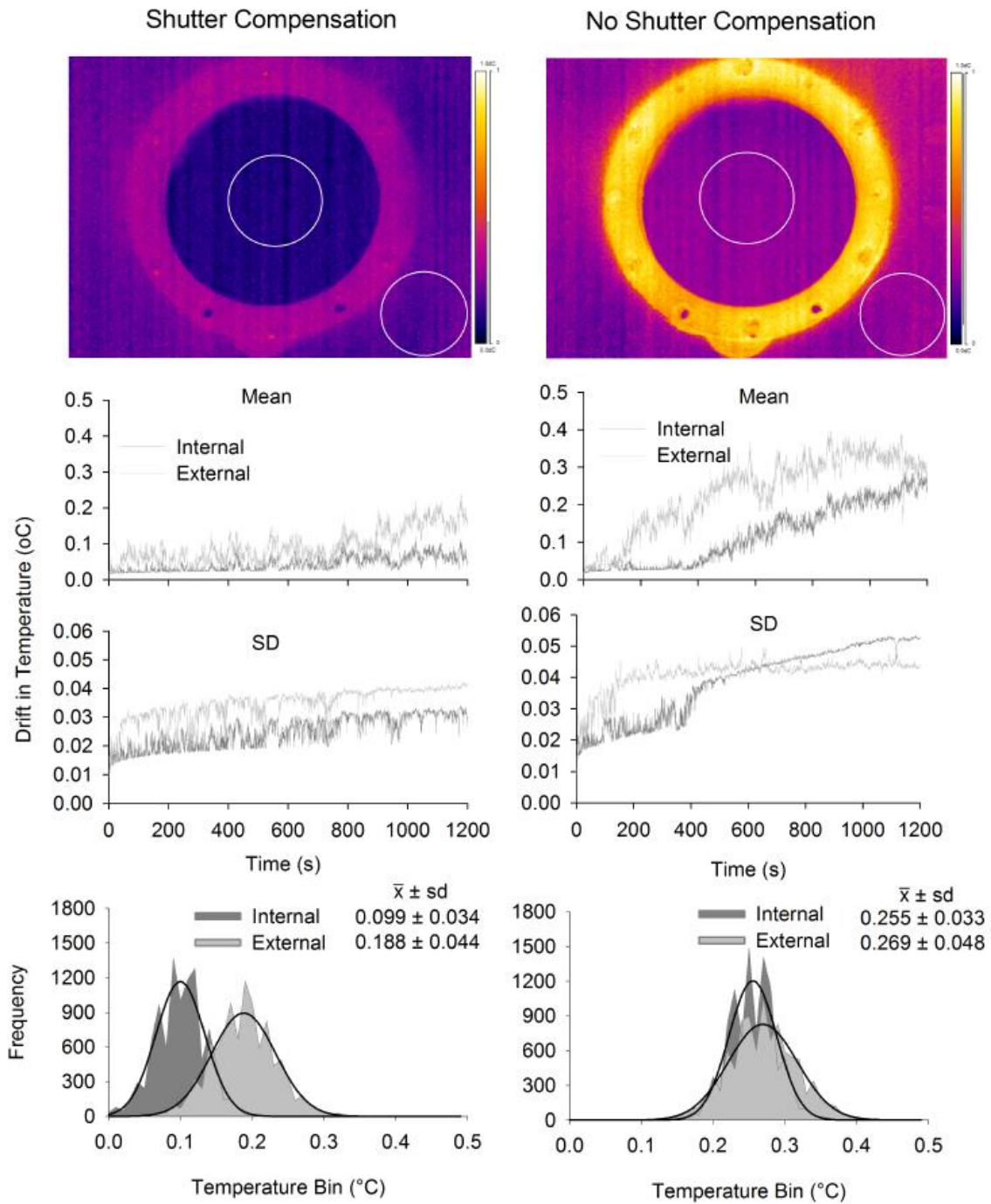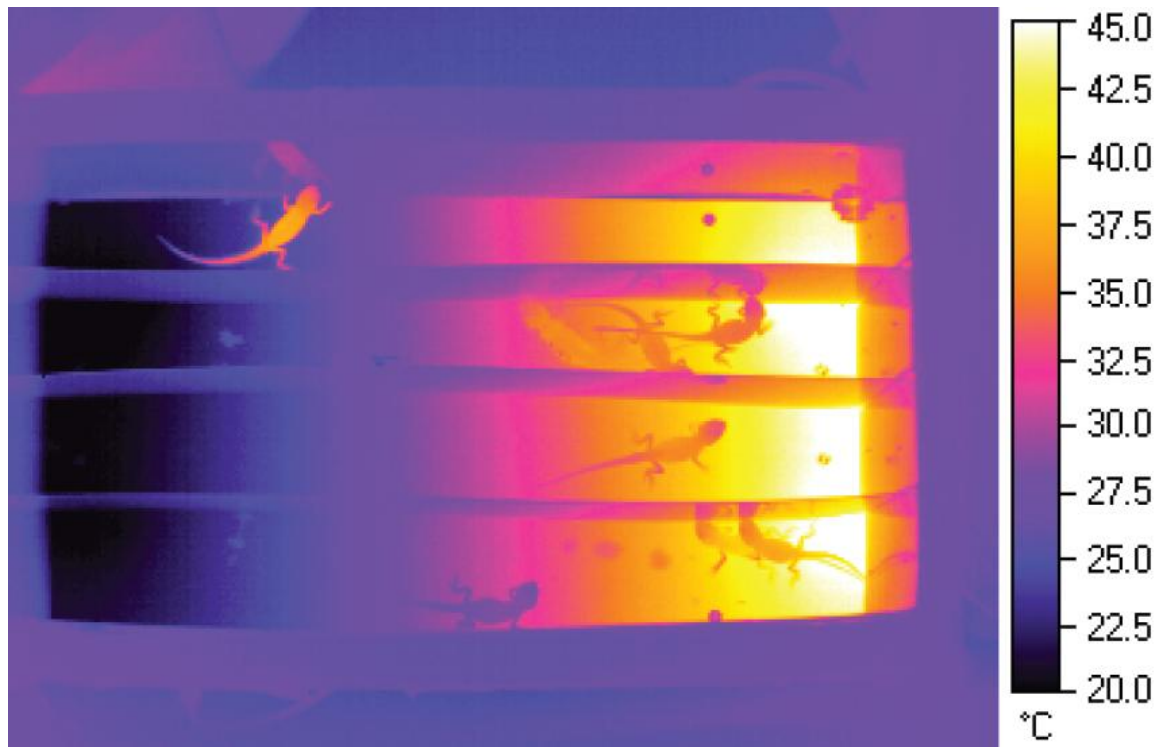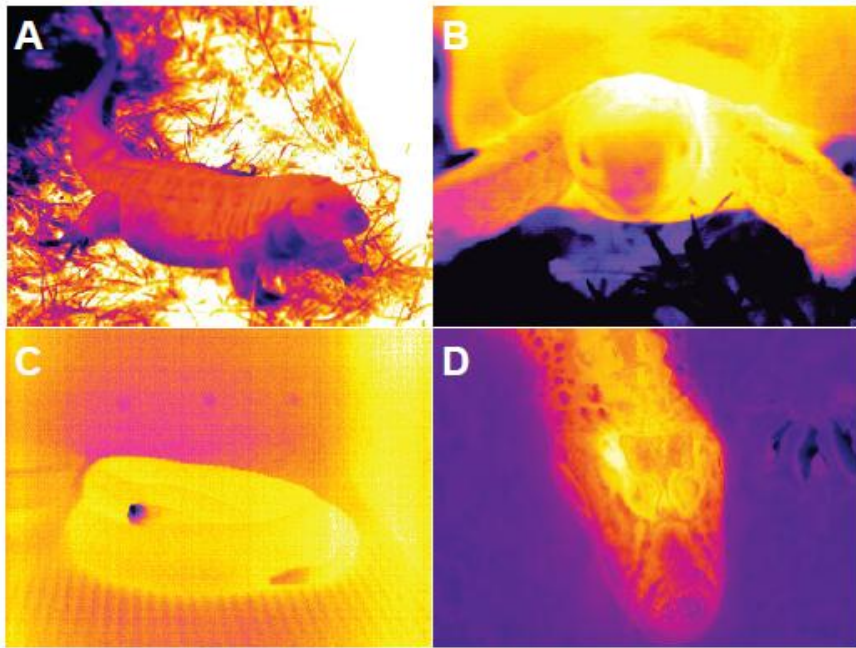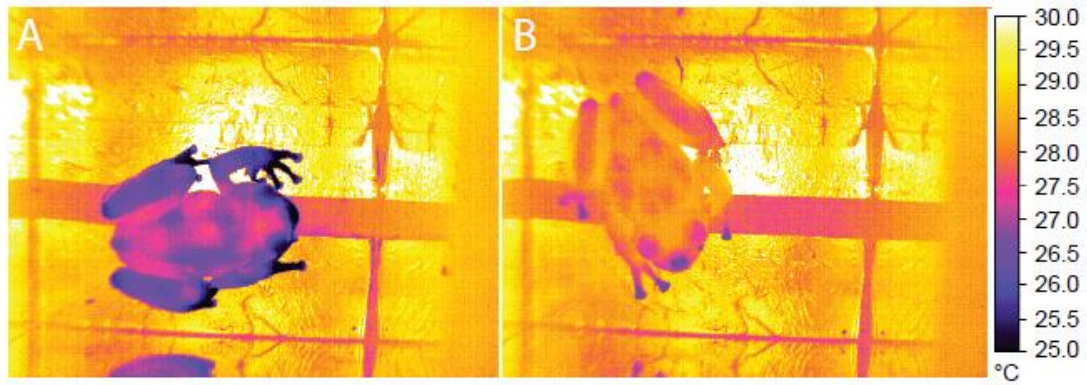


Fig. 10

Fig. 11

Fig. 12

Fig. 13

Fig. 14

Fig. 15